(2)

DOCTORAL THESIS

Model Studies on Non-Heme Iron Enzymes.

EPR Characterization of Reaction Intermediates.

Satoshi Fujii

Division of Chemical Physics
Department of Chemistry
Faculty of Science
Kyoto University
1992

Contents

Preface

The living thing consists of essential molecules such as nucleic acids, amino acids, proteins, lipids, and sugars. All of these, which are important and indispensable, comprise only six elements, i.e. H, C, N, O, P, and S. In the case of human being, the total amount of H, C, O, and N occupies 96 % of the whole body. If the second group of Na, Mg, K, Ca, P, S, and Cl are included, the ratio exceeds 99 %. However, we cannot maintain our life with these eleven elements only. Among the rest of the elements, there is a group of inorganic elements called 'essential trace elements'.

Several transition metal elements such as Mo, Zn, Fe, V, Cr, Cu, Mn, and Co are the members of this group. Most of them are constituents of enzymes at their active sites, and play important roles in their catalytic cycles. The reactions catalyzed by enzymes are considerably efficient and selective. Why so? In order to answer this question, a lot of efforts have been made, and now, in virtue of the great pioneers, we can understand some biological systems on molecular level. However, the studies of enzyme itself often meet with the difficulty because enzymes are extraordinary large proteins and have diversity in their roles and structures. Furthermore, enzyme reactions are sometimes too fast to investigate their reaction mechanisms in detail. Therefore, model systems which mimic the biological function are often employed in place of enzymes themselves. These approaches through which we study the model systems to elucidate the biological systems are the major part of "Bioinorganic Chemistry'. In fact, the results obtained through the model studies may not be the same as the ones obtained through the enzyme studies, but the model studies selected carefully afford us many valuable information about the real biological systems.

This thesis contains the collected papers and discussions of the author's study at Department of Chemistry, Faculty of Science, Kyoto University during 1988–1992. The aim of this thesis is to clarify the reaction mechanisms of the non-heme iron enzymes with activated oxygen and the dioxygen activation mechanism catalyzed by non-

heme iron enzymes through the model studies. Chapter I gives a general introduction to this thesis, which afford the background and the significance of the studies. In Chapter II, the experimental procedures and the theoretical background for the analyses of the experimental results obtained are described. Chapter III is dealt with the superoxide dismutase model system. In this chapter, the structures of the peroxide complexes are revealed. The detection of the metal-bound superoxide anion is also demonstrated. Chapter IV shows the results of the model studies on catechol dioxygenases. In this chapter, an important role of the Fe(III)-monodentate catecholate intermediate is discussed. In Chapter V, attempts are made to find the correlation between the coordination environment of the non-heme ferric complexes and the EPR parameters on the basis of the observations.

As a whole, the present studies aim at elucidating the reaction mechanisms of the enzymes. Enzymes are great catalysts with which artificial catalysts can hardly compete. It is a great pleasure for the author if he can appreciate the greatness of nature and contribute the illumination of the mystery of life through these studies.

Acknowledgments

The present thesis is the summary of the author's study from 1988 to 1992 at the Division of Chemical Physics of Department of Chemistry of Faculty of Science of Kyoto University. The author is indeed happy to express his great sincere acknowledge to Professor Noboru Hirota for his warm encouragement and criticism. The author also wishes to express his sincere gratitude to Associate Professor Hiroaki Ohya for his cordial and tolerant guidance throughout the course of this study.

It should be emphasized that the studies in this thesis have been supported by many investigators and colleagues. Grateful acknowledgment is made to Professor Akira Nishinaga. He gives a great knowledge of organic chemistry, especially of oxidation of catechols to the author. Heartily thanks are also made to Messrs. Kazushige Maruyama and Takeshi Ootsuki for their kind help for NMR measurements. The author wishes to express his sincere thanks to Professor Kazuhiko Ishizu for his adequate advice. Grateful acknowledgment is also made to Dr. Kunihiko Tajima for his pertinent advice of the reaction of peroxides. The author wishes to express his great gratitude to Dr. Ikuko Ueno. She gives a lot of biological knowledge to him. He also express his gratitude to Professor Keisuke Makino and Mr. Takuya Hagiwara. He is greatly indebted to Messrs. H. Nishishita and N. Kasugai for low temperature experiments using liquid helium and nitrogen. He wishes to express his great gratitude to the fellow members of this laboratory; especially for Dr. Kouichi Fukui and Dr. Satoru Nakashima.

Finally, the author would like to express his greatest gratitude to his parents for their continuous and warm encouragement.

December, 1992
Kyoto
Satoshi Fujii

I. General Introduction

Metalloproteins and metalloenzymes play important roles at various stages in living things, e.g. electron transfer, oxidation, reduction, and oxygen carriage. Most of these functions can be attributed to the metal ions at the active centers of the proteins and enzymes. Although several transition metal ions known as 'essential trace elements' are contained in them, the iron ion is one of the most prevalent and important one. Especially, since the birth of the first aerobe, cyanobacterium, or before then, iron-containing proteins which interact with O_2 and iron-containing enzymes which catalyze the reactions concerned with O_2 have been developed extensively.

Table I-1 shows the examples of iron-containing proteins and enzymes. In general, these are divided into two groups by the ligand type of iron centers. One group is called heme protein and enzyme, e.g. hemoglobin and cytochrome P-450. This class of proteins and enzymes (hemoproteins) are characterized by porphyrin ligand in their active sites. Hemoproteins have been investigated extensively through the studies on proteins themselves and on model porphyrin complexes, and their functions have been well understood. The other group is called non-heme proteins and enzymes, e.g. ferredoxin and superoxide dismutase. This class of proteins and enzymes have no porphyrin ligand. The active sites of these consist of iron centers, the residues of amino acids such as histidine, tyrosine, aspartic acid, and cysteine, and sometimes water. Recently, the studies of these non-heme iron proteins and enzymes have been made vigorously. However, compared to hemoproteins, our understanding of the non-heme iron proteins and enzymes is rudimentary because of the paucity of information about their structures, functions, and so on.

Among various functions of iron-containing proteins and enzymes, the author takes main interest in the non-heme iron enzymes which catalyze the reactions concerned with O_2 (upper right part of Table I-1), especially in superoxide dismutase and catechol dioxygenases. Superoxide dismutase (SOD), an enzyme which

Table I-1. Iron-Containing Proteins and Enzymes

Biological function		Proteins / Enzymes heme	non-heme
Oxygen transport	mono	hemoglobin myoglobin	
or storage	di		hemerythrin
Oxygenase	mono	tryptophan 2,3-dioxygenase	catechol dioxygenases
		cyt. P-450	lipoxygenase
			aromatic hydroxylases
	di		methane monooxygenase
Oxidase	mono	cyt. c oxidase	
	octa		xanthine oxidase
Defence against oxygen toxicity	mono	catalase peroxidase	superoxide dismutase
Electron transfer	mono	cyt. a,b,c	rubredoxin
	poly		ferredoxin
Reduction of ribo- to deoxyribonucleotides	di		ribonucleotide reductase
Iron transport			transferrin
Iron storage	poly		ferritin
			hemosiderin
Unknown	di		purple acid phosphatases

catalyzes the dismutation of superoxide radicals to hydrogen peroxide and oxygen, plays an important role in the protection of cells against the destructive effects of the superoxide radical.[1] Catechol dioxygenases (CTD) catalyze the oxidative cleavage of catechols and serve as central enzymes in biodegradation of aromatic compounds.[2] In spite of the importance of these enzymes, there still remain a lot of problems to be solved.

In this thesis, we attempt to clarify the intermediate structures of these enzymes and the reaction mechanisms of these enzymes by using model complexes, FeEDTA† as a model for FeSOD, and FeNTA, Fe(salen)Cl, and Fe(sal-L-aa)Cl for CTD. It is essential for understanding the nature of enzymes to know the intermediate structures and the reaction mechanisms. The intermediates appearing in the enzymatic reactions are often very unstable and short-lived, so that it is difficult to detect them directly by means of any measurements. The utilization of model complexes sometimes overcomes this difficulty and makes it possible to detect the intermediates directly. Even using model complexes, however, the reaction intermediates are also unstable and short-lived. In order to detect such transient species directly and to investigate the structures of them, EPR spectroscopy is one of the most strong method because it is very sensitive to paramagnetic species and affords the information about the iron ion in the reaction center.

The aim of this thesis is twofold. One is to elucidate how the coordination chemistry of the non-heme iron enzymes relates to the enzymatic function through the model studies. Especially, the role of iron center and the effect of the ligand are considered. The other is to seek for the relation between the coordination environments of the non-heme iron complexes and the EPR parameters. As for the heme enzymes and the model complexes which have a commom porphyrin ligand, their axial ligands can be deduced from the parameters teteragonality and rhombicity calculated easily from the observed g

† Abbreviations: EDTA, ethylenediaminetetraacetic acid; NTA, nitrilotriacetate; salen, *N,N'*-ethylenebis(salicylideneamine); sal-L-aa, N-salicylidene-L-amino acid; EPR, elelctron paramagnetic resonance

values. Taking advantage of the relation, the studies of heme enzymes and model complexes have been developed extensively. Although a lot of efforts have been made to interpret the EPR spectra of non-heme iron complexes and enzymes, such correlation has not been established. Once it is established, the information on the coordination environment should be derived from the EPR spectra more easily. In the last chapter, the attempt to find such correlation will be discussed.

II. Experimental Section

II–1. Materials

FeSOD Model System.

NaFeEDTA·3H_2O was purchased from commercial sources and used as received. The complex synthesized according to a published procedure[3] was also used. Na_2EDTA, 30 % H_2O_2, NaOH, and *t*-BuOOH† were of the highest quality commercially available and were used without further purification. An alkyl peroxide, (*n*-BuOOH) was offered by Professor Ishizu of Ehime University.

CTD Model System.

Three kinds of complexes were used in this system. FeNTA$(H_2O)_2$,[4] [Fe(salen)Cl]$_2$,[5] Fe(sal-L-aa)Cl[6] were prepared according to literature procedures. For Fe(sal-L-aa)Cl, the complexes containing four amino acids, alanine, valine, phenylalanine, and histidine were synthesized. $DBCH_2$ and $catH_2$ were recrystallized from hexane and toluene solution, respectively. 3-$MecatH_2$ and 4-$MecatH_2$ were sublimed under reduced pressure. $4NO_2catH_2$, $pBCH_2$, $PCAH_2$, and $HPCAH_2$ were used as received. All other reagents and solvents were of the reagent grade.

---

† Abbreviations:*t*-BuOOH, *tert*-butyl hydroperoxide; *n*-BuOOH, *normal*- butyl hydroperoxide; $DBCH_2$, 3,5-di-*tert*-butylcatechol, $catH_2$, pyrocatechol; 3-$MecatH_2$, 3-methylcatechol; 4-$MecatH_2$, 4-methylcatechol; $4NO_2catH_2$, 4-nitrocatechol; $pBCH_2$, 4-*tert*-butylcatechol; $PCAH_2$, protocatechuic acid (3,4-dihydroxybenzoic acid); $HPCAH_2$, homoprotocatechuic acid (3,4-dihydroxyphenylacetic acid)

II–2. Physical Measurements

EPR Spectroscopy

EPR measurements were carried out with a JEOL FE-3X spectrometer equipped 100-kHz field modulation at 77 K and 4.2 K. EPR spectra at 77 K were obtained with a liquid nitrogen Dewar flask by slow immersion of sample tubes in liquid nitrogen. Temperatures below 77 K were controlled with an Air Product Model LTR-3-110 cryostat. The microwave frequency (X–band) was measured with a Takeda Riken TR5211A frequency counter. Cr(III) in MgO (g=1.9800) was used as a standard g marker. Fe(III)EDTA in Me_2SO (g=9.6 and 4.3) was also used as a calibrant of the magnetic field. The g values of the observed EPR spectra were estimated based on the microwave frequency and the magnetic field calibrated by these three resonances (9.6, 4.3, and 1.98).

Optical Measurements

Optical spectra were recorded on an Ohtsuka Electronic Co. Ltd., MCPD-1000 28C spectrophotometer. By using this apparatus, EPR and absorption spectra can be measured simultaneously for the same sample in the same quartz tube. Absorption spectra were also recorded by using a Shimadzu UV-3000 double beam spectrometer in Instrumental Analytical Center of this department.

NMR Spectroscopy

^{1}H-NMR and ^{13}C-NMR spectra were obtained in $CDCl_3$ and were recorded on a Varian Unity 300 spectrometer. Tetramethylsilane was used as an internal reference. NMR measurements were performed at Osaka Institute of Technology.

Electrochemical Measurements

Electrochemical measurements were obtained in Me_2SO solution with 0.1 M tetra-*n*-butylammonium tetrafluoroborate as electrolyte on a PAR Model-173 potentiostat. A three-electrode system consisting of a Au working electrode, and a Au counter electrode, and a Ag^+/Ag reference electrode was used. The ferricinium/ferrocene couple was used as an internal standard (calibrated +400 mV vs. NHE†).

II–3. Theoretical Survey of Analyses

In this thesis, we are mainly concerned with the EPR spectra of non-heme ferric complexes. The EPR spectra of transition metal ions reflect the electronic structures of the ions. In this section, therefore, we will survey the electronic structures of the transition metal ions.

Electronic Structure of Transition Metal Ion[7]

Now consider the transition metal ion placed in an applied field **H**. The total Hamiltonian of this ion is written as follows;

$$\mathcal{H} = \mathcal{H}_0 + V_{rep} + V_{C.F.} + \sum_i \xi\, l_i \cdot s_i + \sum_i \beta(\mathbf{L} + g_e\mathbf{S})\cdot\mathbf{H} \qquad \text{(II-1)}$$

The first term represents the kinetic energy of electrons and the Coulomb attractive energy between electrons and nucleus. The second and the third term mean the Coulomb repulsion between electrons, and potential of the crystal field constructed by the ligands respectively. The fourth term denotes the spin-orbit coupling (V_{SO}). The fifth term is the Zeeman energy of electrons. In eq.II-1, the hyperfine interaction is omitted because we treat only iron ion whose nuclear spin equals zero. Other interactions such as nuclear Zeeman term and nuclear quadrupole interactions are also omitted because their magnitudes are negligible compared to those of the terms in eq.II-1.

† Abbreviation: NHE, normal hydrogen electrode

When we consider the transition metal ions under some crystal field, $\mathcal{H}_0$ is larger than other terms and the Zeeman term is the smallest of all at an experimental range (0~1 T). Consequently, electronic configurations of transition metal ions depend on the order of the magnitude of V_{rep}, $V_{C.F.}$, V_{SO}. Typical three cases are as follows with their representatives:

(1) $V_{rep} \gg V_{SO} \gg V_{C.F.}$ (Weak field)
Case for the rare-earth metals.

(2) $V_{rep} \gg V_{C.F.} \gg V_{SO}$ (Intermediate field)
Case for the iron group.

(3) $V_{C.F.} \gg V_{rep} \gg V_{SO}$ (Strong field)
Case for 'covalent bond type' complexes.

The ferric high-spin complexes we treat in this study belong to the case (2) where V_{rep} and $V_{C.F.}$ are of the same order. In this case, two approaches can be adopted to explain the electronic configuration. One is weak-field approximation and the other is strong-field approximation. For high-spin complexes, the former approach is favorable.

In the weak-field approximation, LS-multiplets are first produced by V_{rep} (^6S for d^5). Next, each multiplet is split into several levels $|S\Gamma M\gamma\rangle$ by crystal field, where γ is a base of an irreducible representation of Γ under the symmetry around the metal. If the splitting by the crystal field is much smaller than the energy separation between LS-multiplets, then eigenfunction of the split levels is written as

$$|S\Gamma M\gamma\rangle = \sum_i C_i |SLM_S M_L\rangle \qquad \text{(II-2)}$$

where the coefficients C_i are determined by the crystal field.

Since the spin-orbit coupling and the Zeeman term are usually smaller than V_{rep} and $V_{C.F.}$, we can treat these two terms with perturbation theory. Within a LS-multiplet, we can rewrite $\sum_i \xi l_i \cdot s_i$ in eq.II-1 as $\lambda \mathbf{L}\cdot\mathbf{S}$. Accordingly, effective Hamiltonian is

$$\mathcal{H} = \lambda\, \mathbf{L}\cdot\mathbf{S} + \beta(\mathbf{L} + g_e\mathbf{S})\cdot\mathbf{H} \qquad \text{(II-3)}$$

When the symmetry of the ligand field is low enough, the ground state has no degeneracy in spatial parts. In such a case, orbital angular momentum is quenched and we can reduce eq.II-3 to an equation including only spin variables.

Due to the perturbation term eq.II-3, other wavefunctions mixed together. Consequently, wavefunction $|S\Gamma M\gamma\rangle$ is no longer orthogonalized. Taken the V_{rep} and $V_{C.F.}$ into consideration, the wavefunction of an arbitrary level is written as

$$\psi = \sum_{n,m} C_{nm} |n\rangle|m\rangle \qquad \text{(II-4)}$$

where ket $|n\rangle$ (n=0, 1, 2, ……, n) and ket $|m\rangle$ (m=–S, -S+1, ……, S) denote the spatial part and the spin part of wavefunction respectively. $|n\rangle$ is orthogonal to the zeroth order Hamiltonian

$$\mathcal{H}^{(0)} \equiv \mathcal{H}_0 + V_{rep} + V_{C.F.} \qquad \text{(II-5)}$$

The first order and the second order perturbation theory give the effective Hamiltonian

$$\mathcal{H} = \beta\mathbf{S}g_e\left(\tilde{\delta} - \lambda\tilde{\Lambda}\right)\mathbf{H} - \lambda^2\mathbf{S}\tilde{\Lambda}\mathbf{S} - \beta^2\mathbf{H}\tilde{\Lambda}\mathbf{H} \qquad \text{(II-6)}$$

where '~' denotes tensor and

$$\Lambda_{\xi\eta} = \sum_{n\neq 0} \frac{\langle 0|L_\xi|n\rangle\langle n|L_\eta|0\rangle}{E_0 - E_n} \qquad \text{(II-7)}$$

$$(\xi, \eta = x, y, z)$$

The last term in eq.II-6 can be neglected since it does not affect the energy levels of electron spins. The tensors can always be reduced to a diagonal form by unitary transformation. Eq.II-6 can be written as

$$\mathcal{H} = \sum_{\xi} \left[\left(g_e - 2\lambda\Lambda_{\xi\xi} \right) S_\xi H_{\xi\xi} - \lambda^2 \Lambda_{\xi\xi} S_\xi^2 \right] \qquad \text{(II-8)}$$

where $\Lambda_{\xi\xi}$'s (ξ = x, y, z) are principal values of the tensor $\Lambda_{\xi\eta}$. Using the relation $S_x^2+S_y^2+S_z^2=S(S+1)$, we can rewrite the second term as

$$-\lambda^2 \Lambda_{\xi\xi} S_\xi^2 = D\left\{ S_z^2 - \frac{1}{3} S(S+1) \right\} + E\left(S_x^2 - S_y^2 \right) \qquad \text{(II-9)}$$

where

$$\begin{aligned} D &= \frac{1}{2}\lambda^2 \left(\Lambda_{xx} + \Lambda_{yy} - 2\Lambda_{zz} \right) \\ E &= \frac{1}{2}\lambda^2 \left(\Lambda_{yy} - \Lambda_{xx} \right) \\ \Lambda_{xx} &+ \Lambda_{yy} + \Lambda_{zz} = 0 \end{aligned} \qquad \text{(II-10)}$$

With the definition

$$g_\xi = g_e - 2\lambda\Lambda_{\xi\xi} \qquad \text{(II-11)}$$

we can obtain the effective Hamiltonian in familiar form,

$$\mathcal{H} = D\left\{ S_z^2 - \frac{1}{3} S(S+1) \right\} + E\left(S_x^2 - S_y^2 \right) + \beta \mathbf{S} \cdot \tilde{g} \cdot \mathbf{H} \qquad \text{(II-12)}$$

called spin Hamiltonian. The first two terms are called zero field splitting and the last Zeeman term. The term *D* and *E* are called the coefficients of 'one-axial' symmetry and 'two-axial' or 'rhombic' symmetry. Quartic terms are also existed if S>2, but these are usually very small, so that they are omitted in eq.II-12. By using this Hamiltonian, we can explain the EPR spectra of various transition metal complexes. The application of eq.II-12 to the ferric high-spin complex (d^5, S=5/2) will be discussed in the following section.

Correlation between Effective g values and *E/D* of S=5/2 System

As shown in the previous section, the terms *D* and *E* arise mainly from the first-order matrix elements of the axial and rhombic fields between the excited quartet states ($^4T_1$) and the ground state ($^6A_1$), and the matrix elements of the spin-orbit coupling between the excited states and the ground state (Scheme II-1). It should be noted that the excited quartet states must have been admixed into one another by the cubic component of the crystal field but that their effect on the ground state does not necessarily reflect the symmetry of the field as is usually supposed.

If *D* and *E* are zero, then an isotropic absorption line with a g value slightly greater than 2 is usually observed.[8] If *D* and *E* are finite but small (0.001~0.1 cm^{-1}), five EPR transitions are observed.[9] In the event that *D* or *E* is large compared to the Zeeman term, $g\beta H$, the eigenstates of eq.II-12 in zero magnetic field are easily found to be three Kramers doublets. For the two limiting cases $D\neq0$, $E=0$ and $D=0$, $E\neq0$, eigenenergies and eigenfunctions can be calculated algebraically. For the first case $D\neq0$ and $E=0$,

$$E_i = D\ m_s^2 \qquad \left(m_S = \pm\frac{5}{2}, \pm\frac{3}{2}, \pm\frac{1}{2} \right) \qquad \text{(II-13)}$$

$$\psi_i = \left| \frac{5}{2}\ m_S \right> \qquad \text{(II-14)}$$

where i denotes the i th Kramers doublet.

For the last case $D=0$ and $E\neq0$,

$$E_i = 0$$

$$\psi_i^{\pm} = \sqrt{\frac{9}{14}} \left[\left| \pm\frac{5}{2} \right> - \sqrt{\frac{5}{9}} \left| \mp\frac{3}{2} \right> \right] \qquad \text{(II-15)}$$

$$E_i = \pm 2\sqrt{7E}$$

$$\psi_i^{\pm} = \sqrt{\frac{5}{28}} \left[\left| \pm\frac{5}{2} \right> \pm \sqrt{\frac{14}{5}} \left| \pm\frac{1}{2} \right> + \sqrt{\frac{9}{5}} \left| \mp\frac{3}{2} \right> \right] \qquad \text{(II-16)}$$

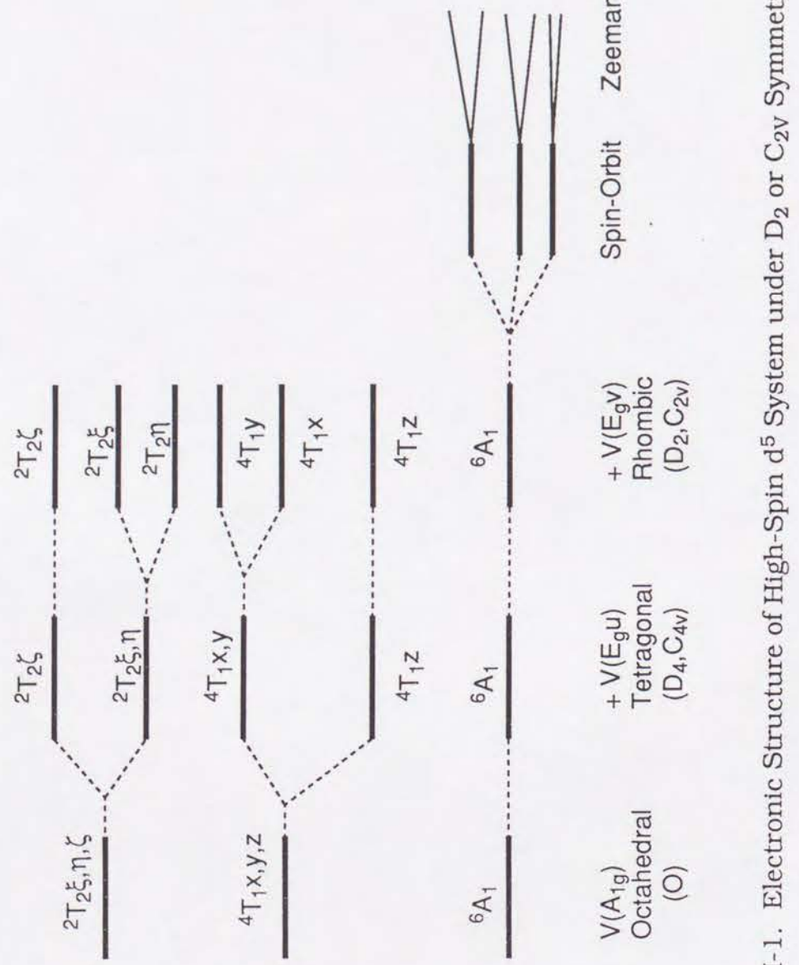

Scheme II-1. Electronic Structure of High-Spin d^5 System under D_2 or C_{2v} Symmetry

It should be noted that these two cases $D\neq0$, $E=0$ and $D=0$, $E\neq0$ can be also represented as $E/D=0$ and $E/D=1/3$ respectively, and that the range of physically distinct values for E/D is restricted to $0\leq E/D\leq 1/3$. The parameter E/D is an index of the field symmetry. If $E/D=0$ represents an axial symmetry, then an increase in E/D represents a departure toward a rhombic symmetry. $E/D=1/3$ represents maximum possible rhombic symmetry with equally spaced Kramers doublets. The effect of a small $E(S_x^2-S_y^2)$ in $E/D=0$ or of a small DS_z^2 in $E/D=1/3$ can be treated with a perturbation theory. However, the difference between the real states and the calculated states cannot be ignored as the perturbation term becomes large. Unfortunately the intermediate case cannot be solved algebraically, so that the direct calculation of the matrix elements of eq.II-12 is required.

	$\left\vert\pm\frac{5}{2}\right\rangle$	$\left\vert\pm\frac{1}{2}\right\rangle$	$\left\vert\mp\frac{3}{2}\right\rangle$
$\left\langle\pm\frac{5}{2}\right\vert$	$\frac{10}{3}D$	$\sqrt{10}E$	0
$\left\langle\pm\frac{1}{2}\right\vert$	$\sqrt{10}E$	$-\frac{8}{3}D$	$3\sqrt{2}E$
$\left\langle\mp\frac{3}{2}\right\vert$	0	$3\sqrt{2}E$	$-\frac{2}{3}D$

The eigenfunctions are written as

$$\psi_i = a_i \left\vert\pm\frac{5}{2}\right\rangle + b_i \left\vert\pm\frac{1}{2}\right\rangle + c_i \left\vert\mp\frac{3}{2}\right\rangle \qquad \text{(II-17)}$$

Figure II-1 shows the plot of the effective g values, g_{eff}, as a function of E/D with D=1.0 cm^{-1}. It should be noted that the effective g values of odd spin system depend on the parameter E/D only, if $D \gg g\beta H$. When $g\beta H$ is comparable to D, the effective g values depend on the parameters both D and E/D. From our calculation, there is no significant change in g values, if $D>$ 0.5 cm^{-1} (Figure II-2).

The complexes used in this study fulfill this condition. Therefore, we can easily evaluate E/D from the observed g values with this diagram.

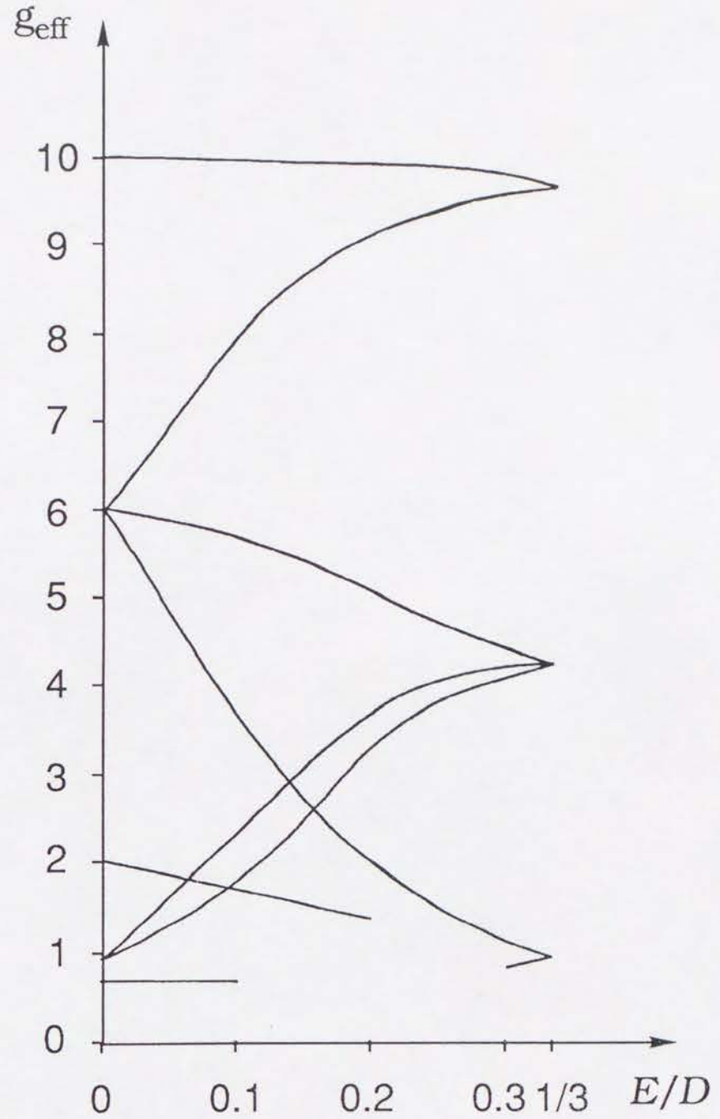

Figure II-1. The effective g values for the S=5/2 spin Hamiltonian plotted as a function of E/D. This diagram shown is calculated 0 to 100 mT with D=1.0 cm^{-1}.

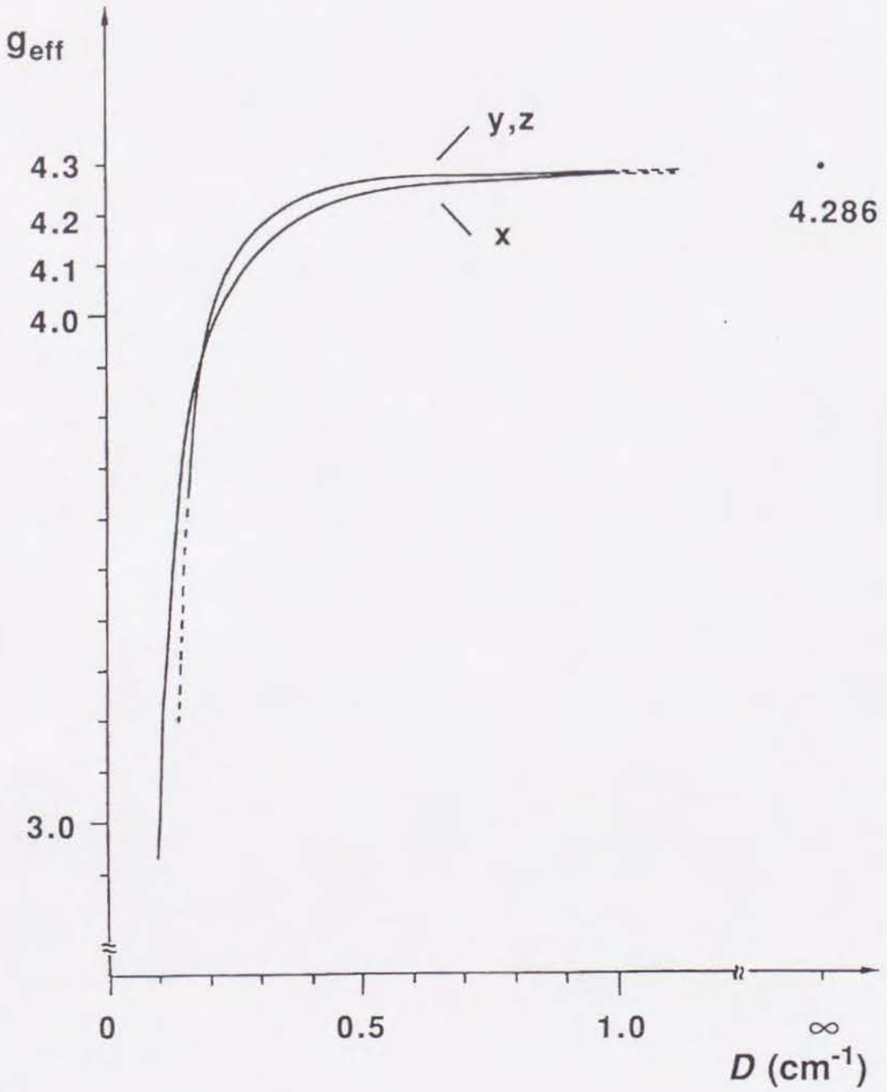

Figure II-2. An example of the D dependence of g_{eff}.
Calculation was made for $E/D = 1/3$.
The g values derived from the middle doublet are plotted. 4.286 was obtained by the second-order perturbation theory.

III. A Study on Fe(III)EDTA System
— As a Model for Iron Superoxide Dismutase —

In this chapter we deal with the reaction of FeEDTA with H_2O_2 and O_2^- as a model reaction of Fe-containing superoxide dismutase (SOD). The toxicity of activated oxygens such as superoxide radical, hydroxyl radical, and peroxide anion is now a serious problem because the activated oxygen is the cause of cancer, myocardial, and other fatal diseases. Hence, it is very meaningful to investigate the reactions of the activated oxygens with enzymes and small model complexes.

III-1. Introduction

Superoxide Dismutase.

SODs are metalloproteins that catalyze the dismutation of superoxide to oxygen and hydrogen peroxide.

$$2O_2^- + 2H^+ \longrightarrow H_2O_2 + O_2 \qquad \text{(III-1)}$$

They are found in microbes, plants, and animals and have been assumed to play an important role in the protection of cells against the destructive effects of the superoxide ion. Three class of SODs have been distinguished according to the metal involved; a Cu/Zn-containing SOD, a Mn-containing SOD, and an Fe-containing SOD. The Cu/Zn-SOD has been most extensively studied by a wide variety of spectroscopic techniques. Mn-SOD and Fe-SOD have, by comparison with the Cu/Zn-SOD, received much less attention.

Fe-SOD was first isolated by Yost and Fridovich in 1973[10] as the third class of SODs. The structure was determined by X-ray diffraction in 1983[11] and at last its active site structure was confirmed in 1990.[12] The molecule is a dimer of two identical subunit with one iron atom per monomer having an overall molecular weight ca. 44000. Two iron atoms at active center are separated by 18 Å and located near the monomer-monomer interface. The iron

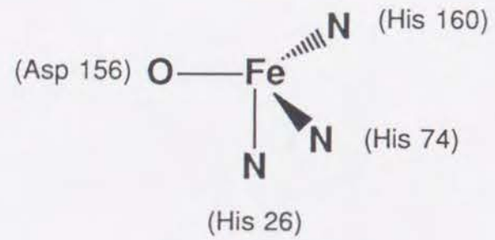

Figure III-1. Schematic drawing of the active site of Fe-SOD from *Pseudomonas ovalis*.[12]

center shows an asymmetric trigonal-bipyramidal structure with the trigonal ligands (two histidines and one aspartate) and the axial ligand (histidine). Another axial coordination position is devoid of bound water molecules or anions. A schematic drawing of the structure of Fe-SOD active site is shown in Figure III-1. Fe-SOD exhibits slightly anisotropic EPR spectrum around g=4.1, the spectrum which is characteristic of a high-spin non-heme ferric system.[10] Several aspects of the mechanism of Fe-SOD are now well-defined.[13] Cyclic inner-sphere oxidation-reduction steps appear to be involved, as shown in eqs.III-1 and III-2. Proton uptake and reduction are concurrent, and the rate-limiting step in catalysis involves proton transfer, possibly in a general-acid assisted breakdown of an Fe(III)-peroxo intermediate.[13a,14]

$$Fe(III) + O_2^- \rightleftharpoons Fe(III)—O_2^- \longrightarrow Fe(II) + O_2 \qquad \text{(III-2)}$$

$$Fe(II) + O_2^- \rightleftharpoons Fe(III)—O_2H^- \rightleftharpoons Fe(III) + H_2O_2 \qquad \text{(III-3)}$$

Model Studies in This Thesis.

In model studies most work has been done with copper complexes. Despite the low toxicity of iron in comparison with copper or manganese, there is very little work reported dealing with iron-containing SOD models.[14,15] Fe(III)EDTA (Figure III-2) is the first reported iron-containing SOD mimic.[15a] Extensive kinetics studies on the Fe(III)/Fe(II)-EDTA catalyzed superoxide dismutation reaction have provided an essential framework for interpreting the enzyme-catalyzed reaction.[14] General-acid-catalyzed breakdown of an Fe(III)-peroxo intermediate is important in the FeEDTA system as well. Fee and co-workers investigated this system and suggested the formation of an intermediate peroxo complex in the catalytic cycle (eqs.III-4~6).

$$Fe(III)EDTA + O_2^- \longrightarrow Fe(II)EDTA + O_2 \qquad \text{(III-4)}$$

$$Fe(II)EDTA + O_2^- \longrightarrow Fe(III)EDTA—O_2^{2-} \qquad \text{(III-5)}$$

$$Fe(III)EDTA + H_2O_2 \rightleftharpoons Fe(III)EDTA—O_2^{2-} + 2H^+ \qquad \text{(III-6)}$$

This peroxide complex, $[Fe(III)\text{-}EDTA—O_2]^{3-}$, was first described by Cheng and Lott in 1956[16] and characterized in considerable detail by others.[3,17-20] However, the mode of dioxygen binding to the ferric ion is still in controversy.[3,14,20]

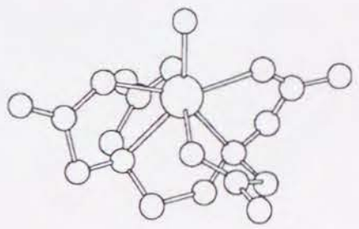

Figure III-2. The structure of $[FeEDTA\text{-}OH_2]^-$. The seven-coordinated ferric ion has a distorted pentagonal-bipyramidal geometry.[21]

The chief aim of this study is to determine the structure of the peroxo complex. In order to fix the structure of the peroxo complex, we investigate the reactions of Fe(III)EDTA with hydrogen peroxide, *t*-BuOOH, and *n*-BuOOH in aqueous solution. There are two possible modes of dioxygen binding to the metal ion. One is an end-on type, and the other is a side-on type. The reason for using alkyl peroxides is that alkyl peroxides can only serves as a monodentate ligand, so that they will bind to the iron only in a monodentate fashion (end-on type).

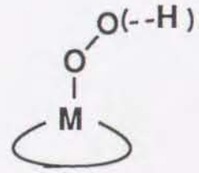

end-on type

side-on type

During the EPR investigations of the reactions, we first succeeded in finding the existence of two types of intermediate peroxo complexes which have different EPR parameters and of a ferrous superoxo complex. We report in this chapter the detection and structural characterization of these complexes. Furthermore, we propose a possible reaction mechanism based on the experimental results obtained.

III-2. Experimental Section

All peroxo complexes were prepared by dissolving NaFeEDTA·3H_2O in H_2O followed by the addition of peroxides to give a solution 2 mM in Fe and 200 mM in peroxides. Na_2EDTA was also added to stabilize peroxo complexes.[18] In this study, a ratio of [FeEDTA]:[Na_2EDTA] =1:5 was employed. In spite of the addition of Na_2EDTA, the peroxo complexes derived from the reaction with H_2O_2 were unstable. Especially the species in neutral pH solution were very unstable, so the samples were frozen rapidly in liquid nitrogen.

III-3. Results and Discussion

Structures of Peroxide Complexes.

In a weak alkaline solution, Fe(III)EDTA behaves as a weak acid.[22,23]

$$[Fe(III)EDTA\text{–}OH_2]^- \rightleftharpoons [Fe(III)EDTA\text{–}OH]^{2-} + H^+ \qquad \text{(III-7)}$$

The EPR spectrum of $[Fe(III)EDTA\text{–}OH]^{2-}$ (**1**) in H_2O (pH 10.0) is shown in Figure III-3a.† The spectrum exhibits a sharp signal at g=4.2 which is characteristic of a high-spin non-heme ferric system. Addition of H_2O_2 to a nearly neutral solution (pH 7.6) resulted in the appearance of a new signal, as shown in Figure III-3b. The sharp signal at g=4.2 appearing in Figure III-3b corresponds to original FeEDTA uncoordinated by the peroxo anion. This is probably due to an equilibrium (eq.III-8) reported by Ringbom et al.[17]

$$[Fe(III)EDTA\text{-}OH]^- + HO_2^- \rightleftharpoons [FeEDTA\text{–}O_2]^{3-} + H_2O \qquad \text{(III-8)}$$

The g values of the new signal (g_1=4.39, g_2=4.15 and g_3=3.90) indicate that this new species (**2**) formed by adding H_2O_2 has high rhombic distortion similar to but distinguishable from **1**. On the contrary, the addition of H_2O_2 to an alkaline solution (pH 11.2) led to a different species (**3**) with a less rhombic distortion, g_1=5.08, g_2=3.81 and g_3=3.37, as shown in Figure III-3c. It is suggested from the comparison of the g values of **3** with those of **2**, that the structure of

† The EPR spectrum of FeEDTA in aqueous solution shows pH dependence. The spectrum exhibits a very broad feature at low pH and becomes sharp as the solution becomes basic. A sharp signal can be observed at neutral region if the solution is frozen rapidly. (See the signal of uncoordinated species in Figure III-3b.) The spectrum at pH 10.0 is chosen for good correspondence to the uncoordinated species in Figure III-3b. The broad signal at pH 7 (not shown) is, of course, different from that of species **2**.

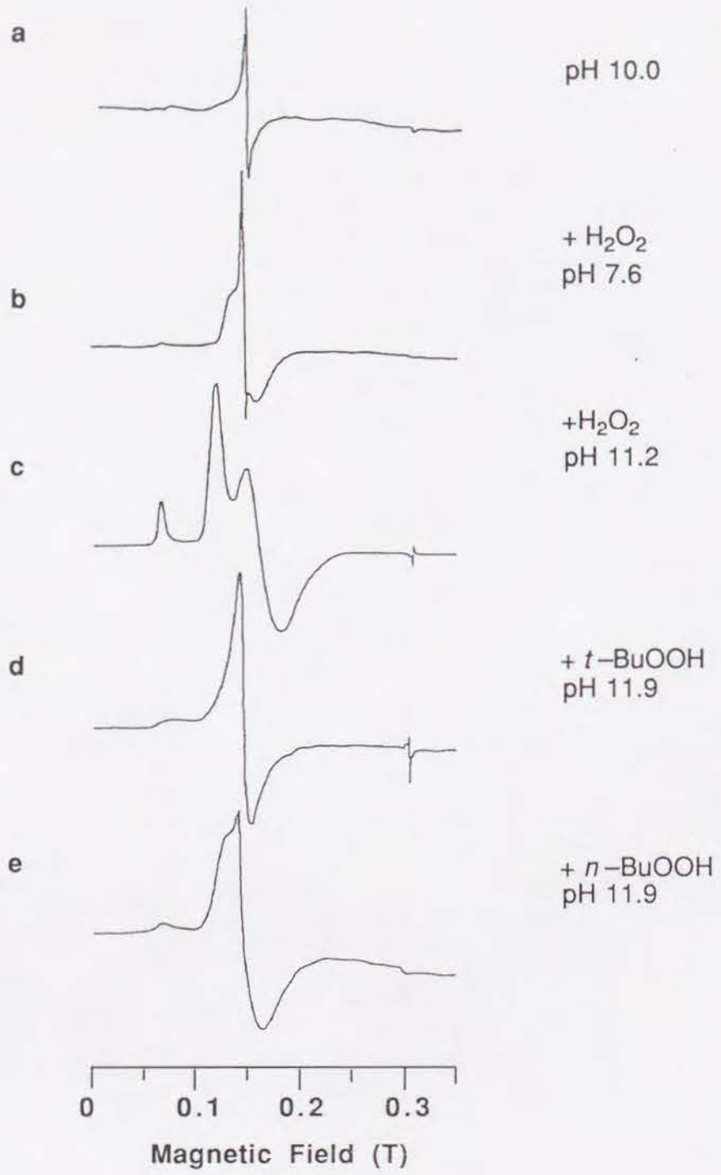

Figure III-3. EPR spectra of FeEDTA complexes in water at 77 K: (**a**) FeEDTA, pH 10.0; (**b**) FeEDTA + H_2O_2, pH 7.6; (**c**) FeEDTA + H_2O_2, pH 11.2; (**d**) FeEDTA + *t*-BuOK, pH 11.9; (**e**) FeEDTA + *n*-BuOOH, pH 11.9.

3 in alkaline solution is different from that of **2** in nearly neutral solution. Indeed, the nearly neutral solution was colorless whereas the alkaline solution was purple (λ_{max}=520 nm, Figure III-4), as has been previously reported.[14,15b,17,18,20]

As the reaction of Fe(III)EDTA with H_2O_2 proceeded, the signal intensity of **3** decreased, and then disappeared. At this stage of the reaction only a small signal due to a trace amount of 1 could be seen. After a while the signal of **1** reappeared and its intensity gradually increased. In the case of the reactions with alkyl peroxides, such intensity change was not observed.

In order to clarify the structure of the intermediate species **2** and **3**, we have tried to react with Fe(III)EDTA with typical organic peroxides. The solutions were prepared at high pH to make organic peroxides serve as anionic ligands, $^-$OOR (generally $pK_a \geq 11.5$ for alkyl peroxides). Figure III-3d shows an EPR spectrum of FeEDTA with *t*-BuOOH in H_2O at pH 11.9. The major component of species formed (**4**) has a little broad line width, the g values being g_1=4.33, g_2=4.18 and g_3=3.98. The signal around g=2 in the Figure is due to the *t*-BuOO$^\bullet$ radical ($g_{//}$=2.03, $g_\perp$=2.008), which is generated from an excess amount of *t*-BuOOH. The spectrum of the FeEDTA—*n*-BuOOH system (5) in alkaline solution (pH 11.9) is shown in Figure III-3e. Its g values, g_1=4.60, g_2=4.18 and g_3=3.75, are similar to those of **2** shown in Figure III-3b.

The observed g values of these complexes are plotted in the g_{eff} vs. E/D diagram (Figure III-5). The g values and the estimated E/D values of these species are summarized in Table III-1. The E/D

Table III-1. EPR Parameters for FeEDTA Complexes with Peroxides

Species	Peroxides	pH	g values			E/D (±0.01)
1		10.0	4.20	4.15	4.14	0.31
2	H_2O_2	7.6	4.39	4.15	3.90	0.29
3	H_2O_2	11.2	5.08	3.81	3.37	0.20
4	*t*-BuOOH	11.9	4.33	4.18	3.98	0.30
5	*n*-BuOOH	11.9	4.60	4.18	3.75	0.28

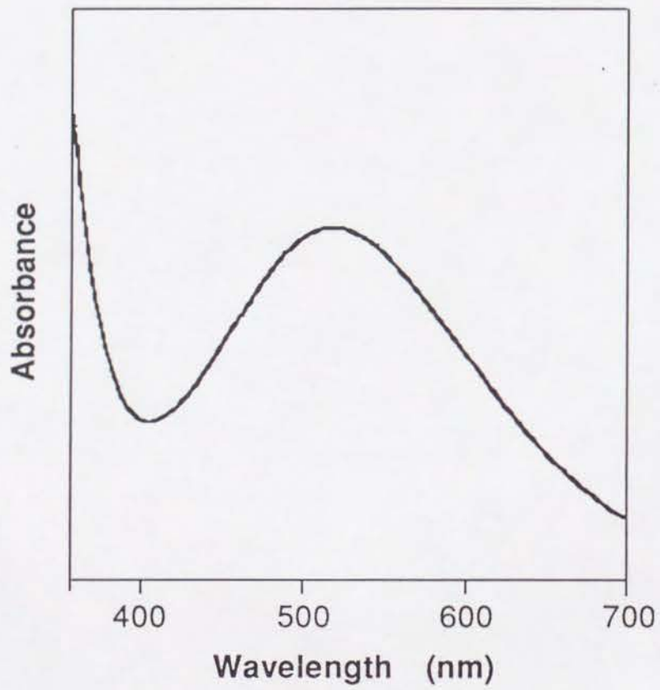

Figure III-4. Absorption spectrum of [FeEDTA–O2]$^{3-}$.

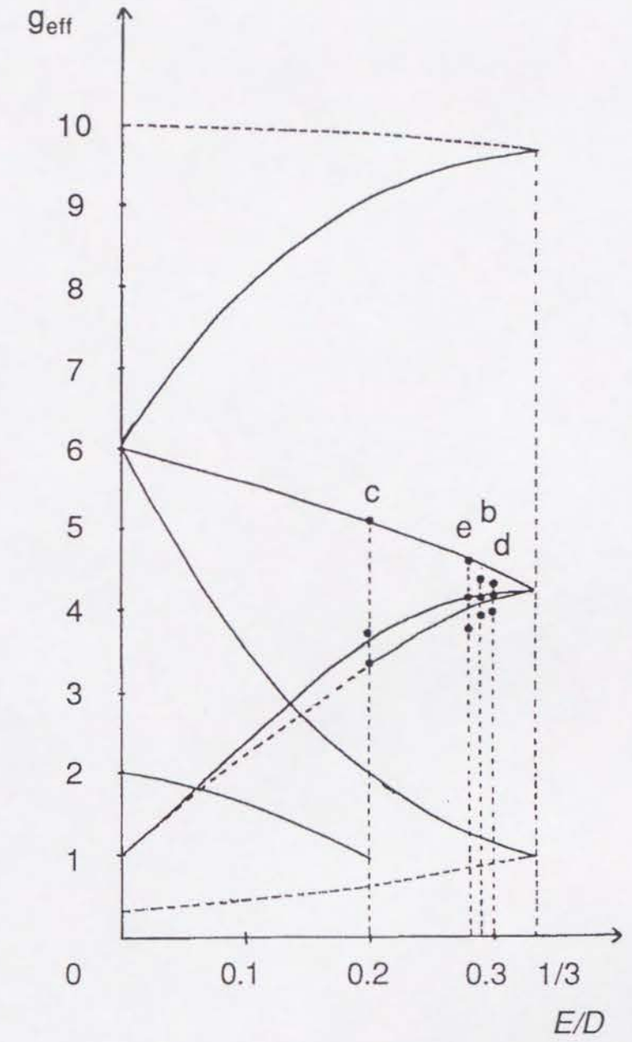

Figure III-5. Plots of the observed g values of the FeEDTA peroxide complexes as a function of *E/D*.

values of species **1**, **2**, **4**, **5** are nearly equal. This fact suggests that the metal environments in these complexes resemble each other. Consequently it is expected that the ferric ions in these species have the same coordination number. Thus, we conclude that the structure of these peroxo complexes is a monodentate or 'end-on' type, $[FeEDTA—^{-}OOR]^{2-}$ (R=H, *t*-Bu and *n*-Bu).

On the other hand, species **3** gives a unique value of E/D = 0.20±0.01. Similar EPR spectra were observed above pH 8 and increased in intensity with pH. According to Francis et al., the intensity of the absorption at 520 nm which characterizes the 'FeEDTA peroxo complex' increased gradually around pH 8 and came to a plateau at pH 10.[20] Thus it is concluded that species **3** corresponds to the 'FeEDTA peroxo complex'. Considering the E/D value of **3**, the structure of **3** is evidently different from those of others. In an alkaline solution, deprotonation of ^{-}OOH is expected and the resultant O_2^{2-} is probably in existence. If O_2^{2-} ligated in an end-on mode, the E/D value of **3** should be nearly equal to those of **1**, **2**, **4** and **5**. Hence it is most likely that the peroxo ligation mode to FeEDTA of **3** is a cyclic or 'side-on' fashion. Our results obtained by EPR measurements support the results of Bull et al.[14] and Ahmad et al.[3]

The chemical precedents for cyclic peroxide structure such as Fe(III)OEP†-peroxo complex,[24] $[Fe(III)TPP(O_2)]^{-}$,[25] $[Ti(IV)TPP](O_2)]^{-}$,[26] $[Mn(III)TPP(O_2)]^{-}$,[27] and $[V(V)O(IDA)(O_2)]^{-}$,[28] have been reported. In particular, the structures of the last two complexes were verified by X-ray crystallography. The precedence for an eight-coordinated complex, diperoxymolybdenum(VI) tetra-p-tolylporphyrin, has also been reported.[29] Since Mo(VI) and Fe(III) have similar ionic radii, Fe(III) may accommodate eight coordination atoms. In addition, the crystal field stabilization energy of high-spin $3d^5$ complexes is zero regardless of coordination number and/or the configuration, so that 'unusual coordination number' is apt to be realized.[30]

† Abbreviations: OEP, octaethylporphyrin; TPP, tetraphenylporphyrin; IDA, iminodiacetic acid

The reason for the decrease in E/D from 0.31 in **1** to 0.20 in **3** is considered as follows. The seven coordinated ferric ion of $[FeEDTA–OH_2]^{-}$ in the crystalline state has a distorted pentagonal-bipyramidal geometry as reported by Lind et al. (Figure III-2).[21] Two nitrogens from amine and three oxygens (one from the water molecule and the others from carboxylates) occupy the pentagonal plane, whereas the remaining two carboxylate oxygens coordinate to the axial position. If a nucleophilic ligand exchange of ^{-}OH with ^{-}OOH results in the 'side-on peroxo complex' $[FeEDTA—O_2]^{3-}$ (species **3**), it is presumably has a distorted hexagonal-bipyramidal geometry. Being occupied by six atoms, crystal field symmetry on the plane may be improved. Therefore the value of E/D, as well as E, is expected to become smaller.

In conclusion, the bound dioxygen in the 'FeEDTA peroxo complex' is in a side-on peroxo configuration. However, our results indicate that the end-on, protonated peroxo complex is also exists in neutral solution. This is the first spectral evidence of the intermediate hydroperoxy complex in this system.

Ferrous Superoxo Complex.

At higher pH (above ca. 12), where the superoxide ion becomes relatively stable, a typical EPR spectrum of O_2^{-} ($g_{//}$=2.060, $g_{\perp}$=2.0069) could be detected (Figure III-6). A signal derived from **3** was also seen with a low intensity in Figure III-6a. These signals suggest two interesting facts. First, through the examination of the reported g values of O_2^{-} which interacts with the metal ions, we found that the value of $g_{//}$ reflects the O_2^{-} environment well.[31] The theoretical equation of $g_{//}$ is

$$g_{//} - 2 \approx 2\left[1/\left\{1+\left(\Delta/\lambda\right)\right\}^2\right]^{1/2} \qquad \text{(III-9)}$$

where λ is the spin-orbit coupling constant of O and is estimated λ= 0.014 eV. Δ is the difference of the orbital energy between π_x and π_y. If a cation links with π_x orbital, the energy of π_x is reduced and Δ becomes larger, so that the value of $g_{//}$ approaches 2. The g

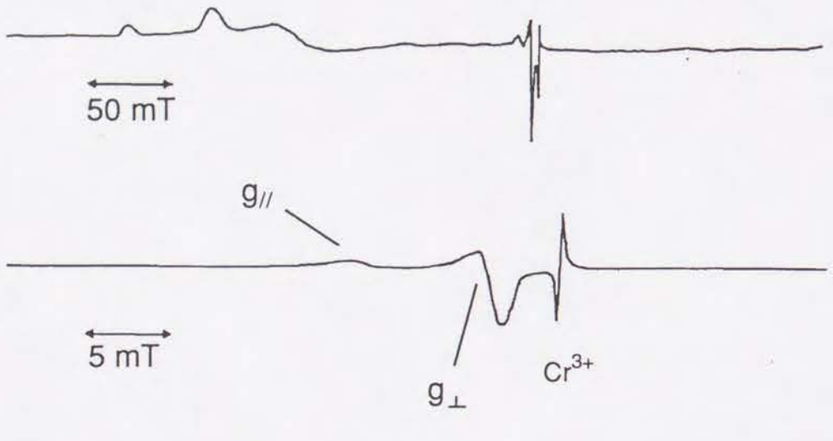

Figure III-6. (a) EPR spectrum of Fe(III)EDTA with H_2O_2 at pH 11.9, 250±250 mT; (b) EPR spectrum of O_2^-, 325±25 mT.

Table III-2. EPR Parameters and Evaluated Δ values of O_2^-

System	$g_{//}$	$g_{\perp}$	Δ (eV)
KCl (crystal)	2.454	1.951	0.06
Na_2O_2	2.175	2.000	0.16
Co(III)-Mb—O_2^-	2.084	2.007	0.34
Fe(III)-xanthine oxidase—O_2^-	2.081	2.001	0.36
Co(III)-P-450$_{cam}$—O_2^-	2.079	2.008	0.37
Co(III)-Hb—O_2^-	2.076	2.003	0.38
Fe(II)EDTA—O_2^-	2.060	2.007	0.47
RSH-Co(III)-TPP—O_2^-	2.04	1.987	0.74

values of O_2^- and the evaluated Δ are listed in Table III-2. Figure III-7 shows the theoretical curves of $g_{//}$ and $g_{\perp}$ against the parameter $\log(\Delta/\lambda)$ reported by Knowles et al.[32] The arrows indicate the $g_{//}$ values observed for O_2^- by various workers and ourselves under different conditions.

Free O_2^- in solution exhibits the signal at $g_{//} \geq 2.10$. If O_2^- has an interaction with the metal ion, $g_{//}$ becomes smaller, e.g. $g_{//}=2.084$ for Co(III)-Mb—O_2^-,[32] $g_{//}=2.081$ for Fe(III)-xanthine oxidase—O_2^-,[31] $g_{//}=2.079$ for Co(III)-P-450$_{cam}$—O_2^-,[33] $g_{//}=2.076$ for Co(III)-Hb—O_2^-[34] (Table III-2). Compared with these $g_{//}$ values, the observed $g_{//}=2.060$ is still smaller. This demonstrates clearly that O_2^- contained in our system interacts with the iron more tightly than other O_2^- in biological systems listed above.

Second a charge transfer process (eq.III-10) is indicated by the decrease of the signal intensity change of **3** and concomitant increase of the Fe(II)—O_2^- complex (see Figure III-3c and Figure III-6a):

$$\text{Fe(III)EDTA—}O_2^{2-} \rightleftharpoons \text{Fe(II)EDTA—}O_2^- \qquad \text{(III-10)}$$

The EPR signal intensity change described in the previous section supports the charge transfer process. This ferrous superoxo complex is a key intermediate in the catalytic cycle both of FeEDTA and FeSOD system (eqs.III-2~III-6). Considering the origin of the shift of

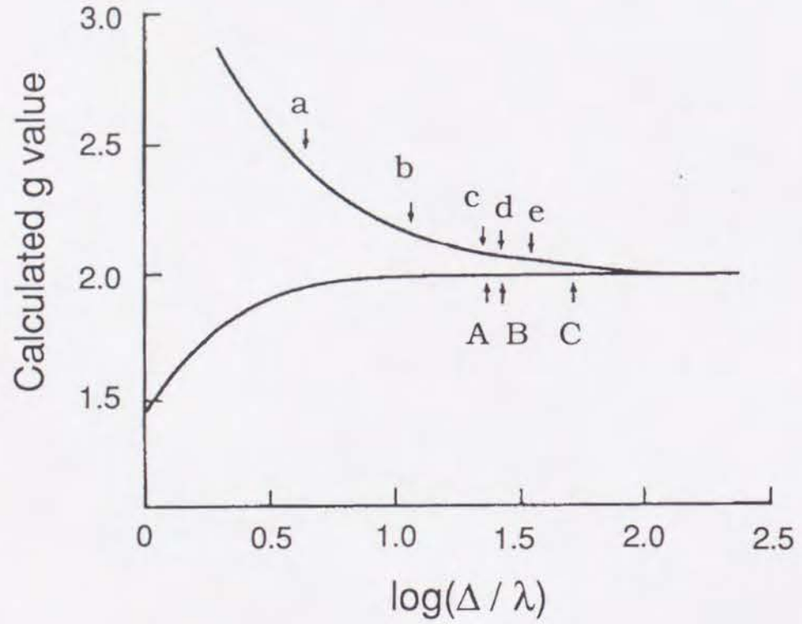

Figure III-7. The observed g values of O_2^-. The curves represent theoretical plots of $g_{//}$ and $g_\perp$ against the parameter $\log(\Delta/\lambda)$. The arrows indicate the $g_{//}$ values observed for O_2^- by various workers under differing experimental conditions. a, O_2^- in irradiated KCl; b, in Na_2O_2; c, from Co(III)-Mb†—O_2^-; from Co(III)-P-450cam—O_2^-; e, from Fe(II)EDTA—O_2^- (this work); A, from Fe(III)-xanthine oxidase—O_2^-; B, from Co(III)-Hb—O_2^-; C, from RSH-Co(III)-TPP—O_2^-.

† Abbreviations: Mb, myoglobin; Hb, hemoglobin

$g_{//}$, it is most likely that the mode of superoxo coordination is in an end-on fashion.

Reaction Mechanism.

In order to examine the reaction mechanism, the reactions of eqs.III-4 and III-5 were also investigated by EPR. The reactions carried out under adequate conditions were traced by EPR. The results obtained support the reactions of eqs.III-4 and III-5.

On the basis of our observations, we propose a possible reaction mechanism as follows:

$$\text{Fe(III)EDTA} + O_2^- \longrightarrow \text{Fe(II)EDTA} + O_2 \qquad \text{(III-11)}$$

$$\text{Fe(II)EDTA} + O2- \rightleftharpoons \text{Fe(III)EDTA—}O_2^{2-} \qquad \text{(III-12)}$$

$$\text{Fe(III)EDTA} + H_2O_2 \rightleftharpoons \text{Fe(III)EDTA—}O_2H^- + H^+$$

$$\rightleftharpoons \text{Fe(III)EDTA—}O_2^{2-} + 2H^+ \qquad \text{(III-13)}$$

Eq.III-11 is identical with eq.III-4. Considering the charge transfer process, eq.III-10, back-reaction in eq.III-5 also occurs (eq.III-12). The detection of species **2** suggests that the existence of transient state $[\text{Fe(III)EDTA–}O_2H^-]^{2-}$ (eq.III-13). Reactions of eq.III-12 and III-13 are schematically shown in Scheme III-1.

Comparison with SOD.

The mechanism of Fe-SOD is proposed as eqs.III-2 and III-3. Compared with the mechanism of enzyme, our proposed mechanism of FeEDTA system is almost the same except for the participation of side-on peroxo complex. In fact, the EPR spectrum of Fe-SOD in the presence of H_2O_2 shows only intensity change probably due to the reduction of Fe(III)-SOD to Fe(II)-SOD.[13b] Therefore, generation of other paramagnetic intermediate complexes seems to be less possible. Moreover, since Fe-SOD peroxo complex has no absorption maximum around 520 nm, the structure of Fe-SOD peroxo complex cannot be the same with the 'FeEDTA peroxo complex' where the peroxo anion bind to the iron in side-on fashion. However, our results clearly demonstrate the reduction of the iron ion caused by H_2O_2, and the

presence of end-on type hydroperoxo complex. The mode of peroxide binding is presumably in end-on fashion.

III-4. Conclusion

In conclusion the present EPR study reveals following two points.

(1) The bound dioxygen of the 'FeEDTA peroxo complex' is in a side-on peroxo configuration, but a transient end-on hydroperoxo complex also exists.

(2) Fe(III) is reduced to Fe(II) by peroxide anion and forms a Fe(II)EDTA superoxo complex.

In this SOD model system, it is suggested that the iron ion forms a redox process with activated oxygens.

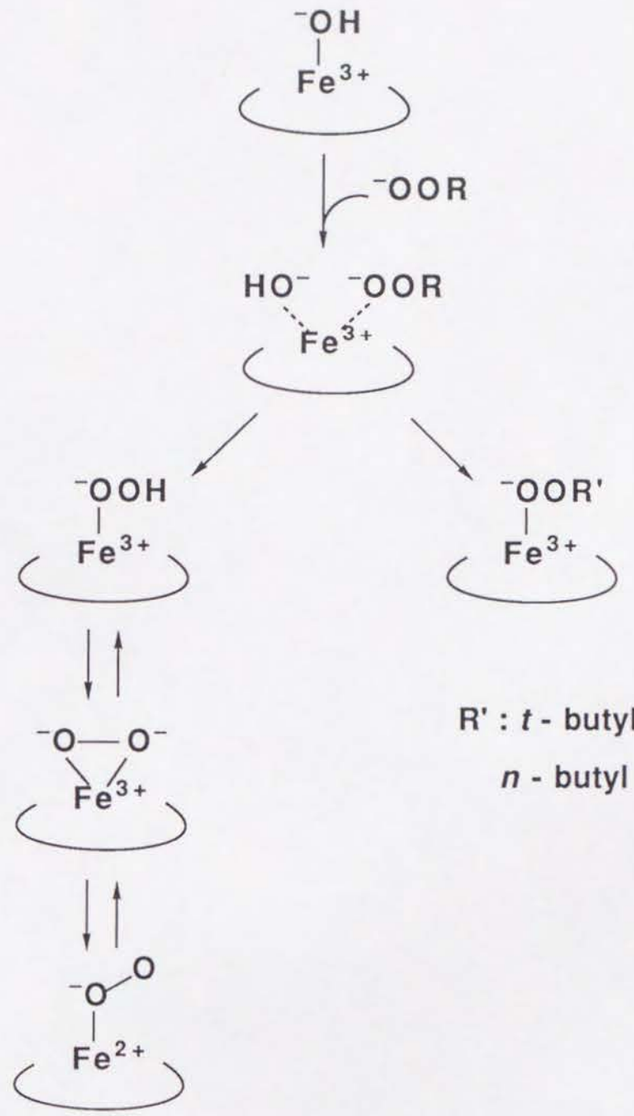

Scheme III-1

IV. Studies on FeNTA, Fe(salen)Cl, and Fe(sal-L-aa)Cl Systems
— As Models for Catechol Dioxygenases —

In this chapter we deal with the catechol dioxygenase model reactions of some non-heme iron complexes with catechols. The aims in this chapter are to determine the structures of intermediate catecholate complexes and to clarify the reaction mechanism of CTD-like reaction. Through the investigations of these model reaction systems, a correlation between the EPR parameters and the coordination environments of the non-heme ferric complexes was noted.

IV-1. Introduction

Catechol Dioxygenases.

Catechol dioxygenases (CTD), non-heme iron enzymes, catalyze the oxidative cleavage of catechol by dioxygen[2] and serve as central enzymes for degrading aromatic compounds. Enzymes are divided into two types according to the style of ring cleavage (Figure IV-1). For example, pyrocatechase (catechol 1,2-dioxygenase) first isolated as catechol dioxygenase by Hayaishi et al.[35] and protocatechuate 3,4-dioxygenase (PCD) are intradiol type enzymes. On the contrary, metapyrocatechase (catechol 2,3-dioxygenase) and protocatechuate 4,5-dioxygenase are extradiol type enzymes. In general, enzymes which catalyze intradiol cleavage have a ferric ion in their active sites, while enzymes which catalyze extradiol cleavage have a ferrous ion.

For experimental reasons, intradiol type enzymes have been extensively studied.[2] Protocatechuate 3,4-dioxygenase (PCD), one of the most characterized of this group, has an active site consisting of trigonal-bipyramidal high-spin ferric center coordinated to two tyrosines (one equatorial, the other axial), two histidines (one equatorial, the other axial), and a water (equatorial) (Figure IV-2).[36]

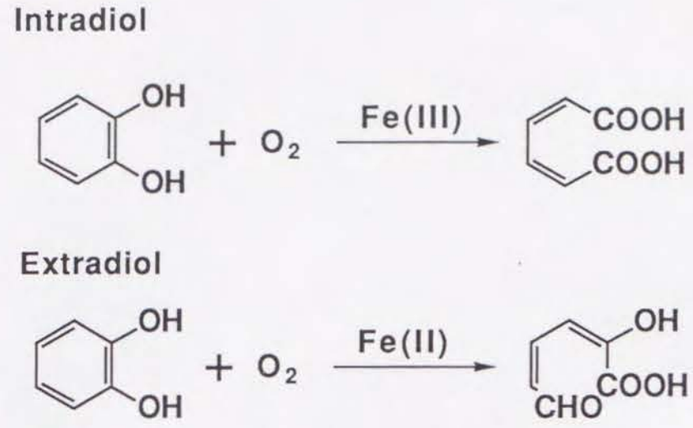

Figure IV-1. Ring cleavage of catechol catalyzed by enzyme

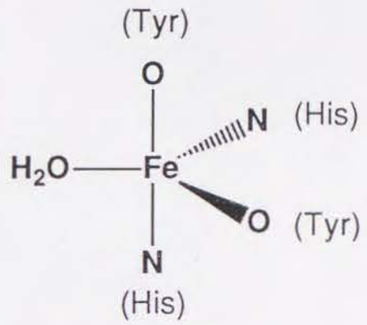

Figure IV-2. Schematic representation of the active site of Protocatechuate 3,4-dioxygenase from *Pseudomonas aeruginosa* [36]

The proposed reaction mechanism involves initial substrate (S) binding to the ferric center of the enzyme (E), followed by the attack of dioxygen on the enzyme-substrate complex (ES). The enzyme-substrate-dioxygen complex (ESO_2) formed is converted to ESO_2^* and then yields the oxygenation products (P) (Scheme IV-1).[37] Mössbauer[38-40] and stopped-flow-kinetic[36,41] studies indicate that the iron remains in a high-spin ferric state throughout the course of the reaction. However, the details of the mechanism have not been clarified yet. Two important problems to be solved for clarifying the reaction mechanism are as follows: First, does the valence of iron change during the catalytic cycle? Second, which intermediate does the molecular oxygen attack?

A number of studies using both enzymes and model complexes have been made to clarify the reaction sequence and some reaction mechanisms have been proposed.[42-45] Especially, the results of model studies are important. Que and co-workers[4] proposed the mechanism involving the Fe(III)(L)-catecholate intermediate (L:tripodal ligands). However, Funabiki and co-workers[46] proposed the Fe(II)-semiquinone intermediate on their $FeCl_3$/bpy/py system. Recently, Que and co-workers also proposed the Fe(II)-semiquinone intermediate on their FeBPG†[45] and FeTPA[47] / $DBCH_2$ systems.

Model Studies in This Thesis.

In order to clarify the above-mentioned unkown points, we first investigated the model reaction of FeNTA and Fe(salen)Cl with catechols by EPR and optical spectroscopies.[48] These complexes have been reported as model complexes of CTD.[43,49] On the basis of the observations, we reported that the valence change of iron depends on the used ligand and that the species attacked by dioxygen is of monodentate catecholate losing both its OH protons.

Next, in order to confirm the results obtained in FeNTA and Fe(salen)Cl systems, we have extended our model studies to Fe(III)

† Abbreviations: BPG, *N,N*-bis(2-pyridylmethyl)glycine; TPA, tris(2-pyridylmethyl)amine; $DBCH_2$, 3,5-di-*tert*-butylcatechol; N T A , nitrilotriacetate; salen, *N,N'* -ethylenebis(salicylidenamine)

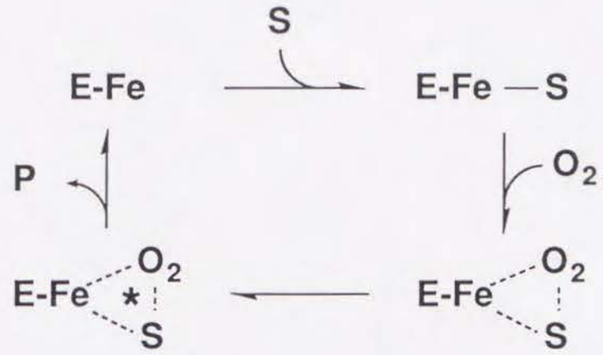

E : Enzyme
S : Substrate
P : Product

Scheme IV-1. Reaction Mechanism of Catechol Dioxygenases

complexes of *N* -salicylidene-L-amino acids, Fe(sal-L-aa)Cl (aa† :ala, val, phe, his) (Scheme IV-2).[6] Since the coordination geometry and the types of ligands (nitrogen/oxygen) differ with used L-amino acids (Scheme IV-2; type **1**: ala, val, phe, type **2**: his) and with NTA and salen, the effects of the geometry and the ligand type can be considered. Moreover, containing L-amino acids in the ligands, these complexes are expected to afford the enzyme-like condition to the iron. Indeed, these complexes react with catechols much faster than NTA and salen complexes. In the Fe(sal-L-aa)Cl system, there was no apparent evidence for the ferric ion to be reduced, and no signal of radical could be observed. Additionally, the ratio of the dianionic monodentate catecholate intermediate to other intermediates having other coordination mode of catecholate is relatively high. These observations suggest that the charge and spin state of iron are unchanged throughout the reaction and that dianionic monodentate catecholate complex is a key intermediate. A comparison of the spectroscopic and reactive properties of these three model systems (NTA, salen, and sal-L-aa) gives useful insights into the reaction mechanism for the enzymes.

IV-2. Experimental Section.

Eight kinds of catechols used in this study are shown in Scheme IV-3. All the samples were prepared under both air and degassed conditions. The sample solutions of FeNTA were prepared by mixing $Fe(NTA)(H_2O)_2$ (2 mM) and catechols, the molar ratios being 1:1, 1:10, and 1:100, respectively, in an aqueous borate buffer (1 part) and DMF (2 part) solution. The use of the borate buffer was to prevent the autoxidation of catechols.[43] The sample solutions of Fe(salen)Cl were prepared by dissolving $[Fe(salen)Cl]_2$ and $DBCH_2$ followed by the addition of potassium *tert* -butoxide (*t*-BuOK). The sample solutions of Fe(sal-L-aa)Cl were prepared by mixing Fe(sal-L-aa)Cl and $DBCH_2$

† Abbreviations: ; sal-L-aa, *N* -salicylidene-L-amino acid; aa, amino acid; ala, L-alanine; val, L-valine; phe, phenylalanine; his, histidine

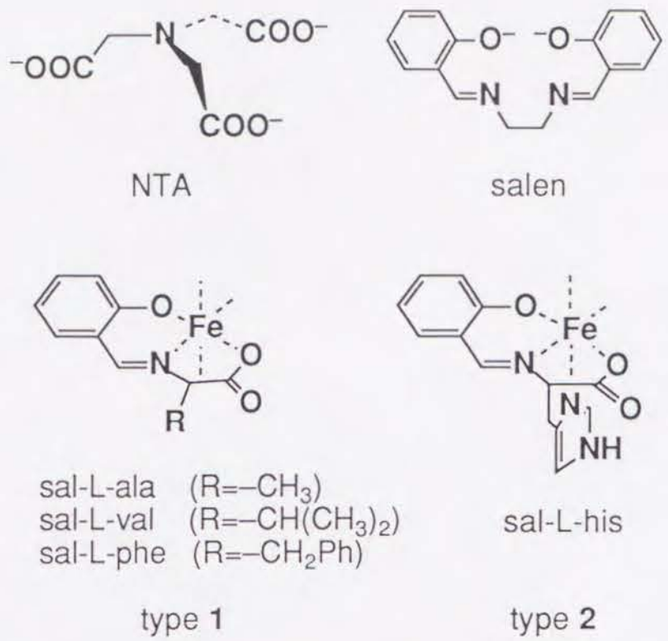

Scheme IV-2. Ligands used in this study

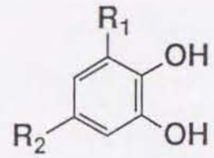

Abbreviations	R_1	R_2
$catH_2$	H	H
$4MecatH_2$	H	methyl
$3MecatH_2$	methyl	H
$pBCH_2$	H	*t*-butyl
$DBCH_2$	*t*-butyl	*t*-butyl
$PCAH_2$	H	COOH
$HPCAH_2$	H	CH_2COOH
$4NO_2catH_2$	H	NO_2

Scheme IV-3. Catechols used in this study.

in an 1:1 molar ratio in MeOH. In order to generate selectively monoanionic catecholate, $DBCH^-$, or dianionic catecholate, DBC^{2-}, 1 equiv. or 2 equiv. of *t*-BuOK was added to the mixture.[6] The oxygenation was carried out under air at room temperature for EPR and optical measurements. In the salen and the sal-L-aa systems, only $DBCH_2$ was used as the substrate, because it exhibits good reactivity for the NTA system.

In this study, product analysis was performed only with the Fe(sal-L-val)Cl system because of fast reaction. Typically, 0.2 mmol of the complex, 2 mmol of $DBCH_2$, and 2 mmol of *t*-BuOK were reacted in 10 mL of MeOH in an oxygen atmosphere at 10 °C for 48 hours. After the reaction was completed, the organic products were extracted with CH_2Cl_2. The products were separated by preparative chromatography on a silica gel plate being developed with CH_2Cl_2.

IV-3. Results.

EPR and Optical Studies.

In this thesis, we investigate the structures of the intermediate catecholate complexes. The possible coordination modes of catecholate are following three types: type I; monodentate $catH^-$, type II; bidentate cat^{2-}, type III; monodentate cat^{2-} (Scheme IV-4).

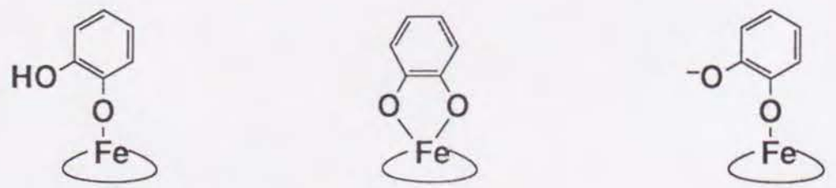

type I type II type III

Scheme IV-4. The modes of catecholate coordination.

FeNTA System.

FeNTA in solution exhibits a typical EPR spectrum of a high-spin non-heme ferric system (g=9.6 and 4.3; E/D~1/3). Upon addition of catechols, the color of the solution changed and new EPR signals appeared due to the formation of the bidentate catecholate complex. EPR spectra of some catecholate complexes, shown in Figure IV-3, are almost the same despite the difference of the substrate catechols. Similar spectra were reported by Cox et al.[50] The value of E/D corresponding to the chelated catecholate species is ca. 0.20 (Table IV-1). The sharp signal at g=4.3 in each spectrum corresponds to FeNTA uncoordinated by catecholate.* It is noted that only DBC complex showed an EPR spectrum derived from two species among the complexes with eight kinds of catechols (Figure. IV-3 C,D). Small signals at g=8.3 and 5.4 arise from minor species with E/D=0.13. This minor species has an different metal environment from the chelated catecholate one (type II; E/D~0.20) and is probably the adduct of the monodentate catecholate dianion (type III), $[Fe(NTA)DBC]^{2-}$, treated later.

Table IV-1. EPR Parameters for FeNTA-catecholate Complexes

catecholate	g values	E/D (±0.01)
cat	9.10,5.08,3.66,3.32	0.20[a]
4Mecat	9.07,4.99,3.68,3.34	0.20
3Mecat	9.09,5.07,3.73,3.37	0.20
pBC	9.05,5.00,3.66,3.30	0.20[b]
DBC	9.10,5.08,3.69,3.38	0.20[a]
	8.3, 5.4	0.13
PCA	9.18,4.93,3.88,3.52	0.22
HPCA	9.07,5.01,3.70,3.31	0.20
4NO2cat	9.24,4.71, ,3.65	0.23

a) In ref. 50, 0.20 and 0.18 are reported for cat and DBC, respectively in DMF/Me_2SO/toluene. b) In ref. 43b, E/D=0.24 is reported pBC in EtOH/borate buffer.

---

* It was confirmed by controlling the amount of the added catechol. The g=4.3 signal is getting smaller as the amount of the added catechol is increasing.

FeNTA System.

FeNTA in solution exhibits a typical EPR spectrum of a high-spin non-heme ferric system (g=9.6 and 4.3; E/D~1/3). Upon addition of catechols, the color of the solution changed and new EPR signals appeared due to the formation of the bidentate catecholate complex. EPR spectra of some catecholate complexes, shown in Figure IV-3, are almost the same despite the difference of the substrate catechols. Similar spectra were reported by Cox et al.[50] The value of E/D corresponding to the chelated catecholate species is ca. 0.20 (Table IV-1). The sharp signal at g=4.3 in each spectrum corresponds to FeNTA uncoordinated by catecholate.* It is noted that only DBC complex showed an EPR spectrum derived from two species among the complexes with eight kinds of catechols (Figure. IV-3 C,D). Small signals at g=8.3 and 5.4 arise from minor species with E/D=0.13. This minor species has an different metal environment from the chelated catecholate one (type II; E/D~0.20) and is probably the adduct of the monodentate catecholate dianion (type III), $[Fe(NTA)DBC]^{2-}$, treated later.

Table IV-1. EPR Parameters for FeNTA-catecholate Complexes

catecholate	g values	E/D (±0.01)
cat	9.10,5.08,3.66,3.32	0.20[a]
4Mecat	9.07,4.99,3.68,3.34	0.20
3Mecat	9.09,5.07,3.73,3.37	0.20
pBC	9.05,5.00,3.66,3.30	0.20[b]
DBC	9.10,5.08,3.69,3.38	0.20[a]
	8.3, 5.4	0.13
PCA	9.18,4.93,3.88,3.52	0.22
HPCA	9.07,5.01,3.70,3.31	0.20
4NO2cat	9.24,4.71, ,3.65	0.23

a) In ref. 50, 0.20 and 0.18 are reported for cat and DBC, respectively in DMF/Me2SO/toluene. b) In ref. 43b, E/D=0.24 is reported pBC in EtOH/borate buffer.

* It was confirmed by controlling the amount of the added catechol. The g=4.3 signal is getting smaller as the amount of the added catechol is increasing.

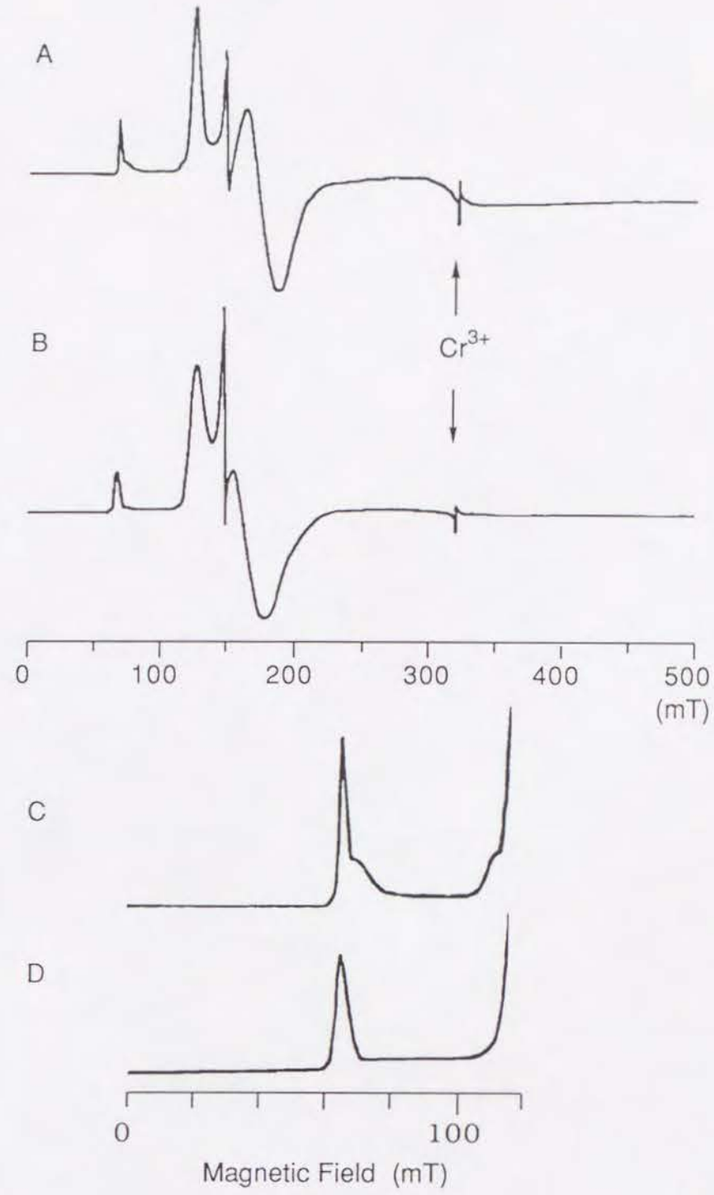

Figure IV-3. EPR spectra of (A), (C) $[Fe(NTA)DBC]^{2-}$ and (B), (D) $[Fe(NTA)]PCA]^{2-}$ in DMF/borate buffer (2:1) solution. The spectra (C) and (D) were enlarged spectra of the low field region of (A) and (B), respectively. Spectra at 4.2 K were obtained at 9.18 GHz with 100-kHz field moculation.

Table IV-2. Catecholate Dependences of Absorption Maxima and Reaction Time of FeNTA-catecholate Complexes in DMF/borate buffer Solution

catecholate	λ_{max} (nm)		Reaction Time (days)	
			R.T.	50°C
$4NO_2$cat	—	470	>10	>10
PCA	379	566	>10	9
HPCA	404	580	>10	9
cat	403	584	10	7
3Mecat	408	604	9	7
4Mecat	415	625	9	7
pBC	416	628	10	7
DBC	440	646	7	3

The visible spectra of the FeNTA-catecholate complexes prepared anaerobically are characterized by two absorption bands (Figure IV-4, Table IV-2). These two bands are assigned to catecholate-to-iron(III) ligand-to-metal charge transfer (LMCT) bands.[4] The lower energy absorption band shifts to higher energy as the nature of the substituents on the catecholate are varied from electron donating to electron withdrawing. However, the spectra of the complexes prepared aerobically exhibit one broad band.

Time-course of the reaction was traced by EPR (Figure IV-5). As the reaction with O_2 proceeded, the signal intensity derived from the chelated catecholate complex decreased gradually, followed by the concomitant increase of that of original FeNTA. From the EPR spectra, the chelated DBC complex with E/D=0.20 almost disappeared in 6 days (Figure IV-5 left). On the other hand, a considerable amount of chelated cat complex with E/D=0.20 still remained 6 days later (Figure IV-5 right). Neither apparent EPR intensity change indicating the reduction of the iron ion from ferric to ferrous nor signal of an organic free radical was observed during the reaction. These observations suggest that the iron remained in the ferric high-spin state and that the reaction time depends on the substrate catechols. Catecholate dependence is also observed in the absorption spectra (*vide infra*). The absorption band in the visible region also diminished corresponding to the change of EPR. Such

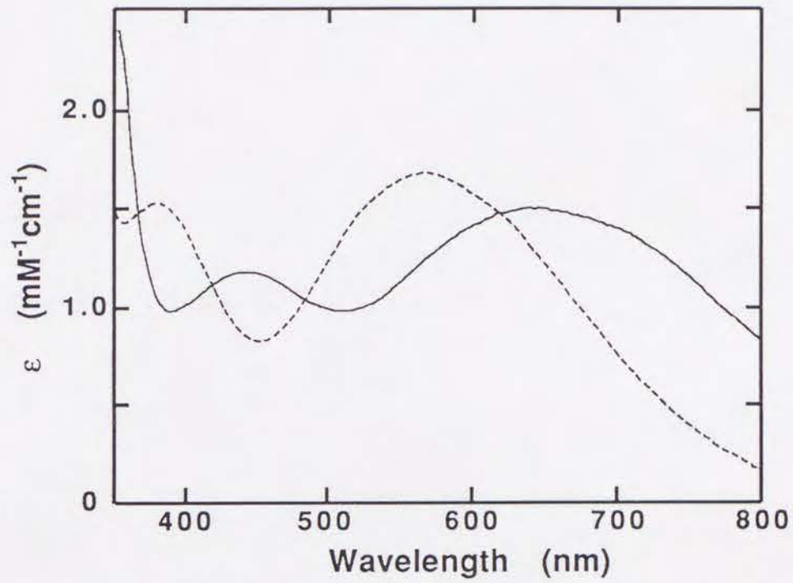

Figure IV-4 Visible spectra of $[Fe(NTA)DBC]^{2-}$ (solid line) and $[Fe(NTA)PCA]^{2-}$ (dashed line). Spectra were obtained anaerobically in DMF/borate buffer (2:1) solution.

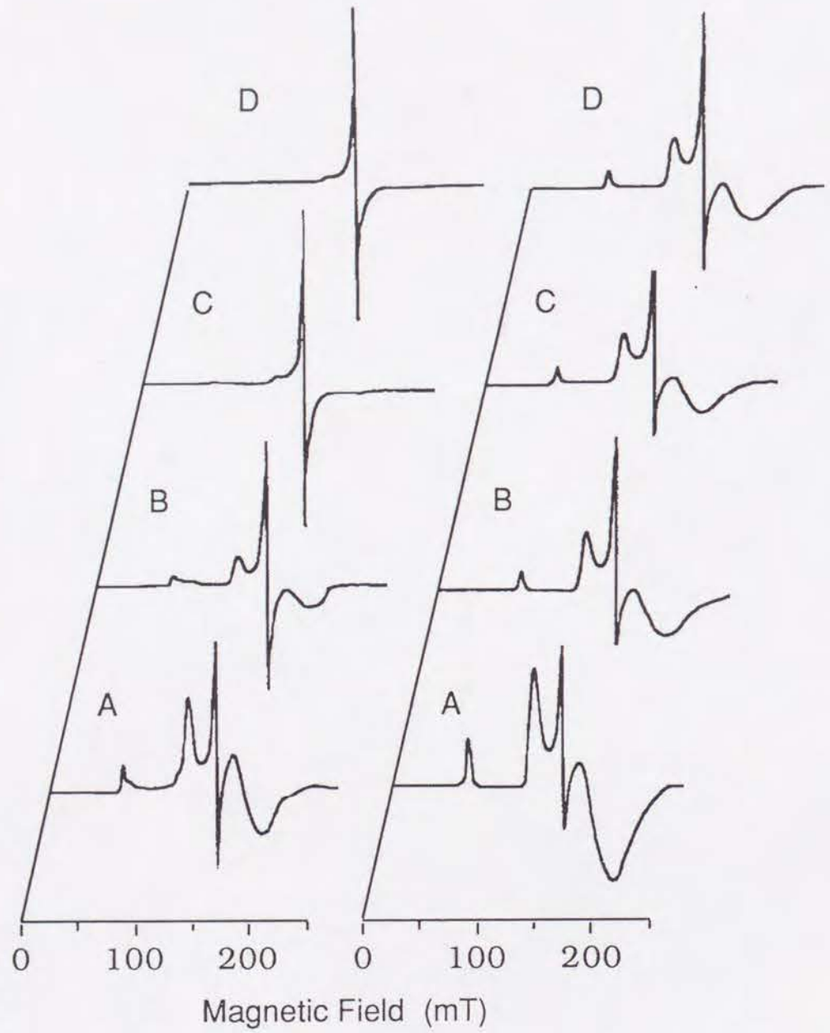

Figure IV-5. Time-course of EPR spectra of $[Fe(NTA)DBC]^{2-}$ (left) and $[Fe(NTA)cat]^{2-}$ (right). The spectra were recorded at (A) 1hour, (B) 2 days, (C) 4 days, and (D) 6 days after addition of catechols.

intensity changes observed in EPR and absorption spectra could not be seen without O_2. At the initial stage of the reaction, however, identical EPR spectra could be observed regardless of the presence of O_2. It suggested that the formation of the catecholate complexes (ES in Scheme IV-1) is the first step of the catalytic cycle.

The reaction times with O_2, in which the characteristic LMCT bands had faded, are listed in Table IV-2. They are consistent with the decay time of the chelated catecholate complexes observed with the EPR (Figure IV-5). It is interesting that the reaction time correlates with the nature of the substituents on the catecholate. The catecholate having more electron-donating substituent reacted faster than the one having less electron-donating substituent. It is worth noting that the DBC complex, solely having a minor species with E/D=0.13, reacted especially fast. This fact suggests that this minor species, monodentate dianionic catecholate complex with the coordination mode of type III, plays an important role in the model reaction.

Fe(salen)Cl System.

Fe(salen)Cl in MeOH showed an EPR spectrum at g=4.3. Fe(salen)Cl and $DBCH_2$ in MeOH did not react without alkaline reagents. Upon anaerobic addition of one or more equiv. of *t*-BuOK, the purple of $[Fe(salen)]^+$ (λ_{max}=510 nm, not shown) changed to green (λ_{max}=620 nm). The sharp resonance at g=4.3, arising from the original Fe(salen)Cl, decreased and the new g=8.75, 5.10, 3.78, and 3.11 (E/D=0.19) resonances appeared. The broad signal at g=4.3 (E/D=0.30) was also observed (Figure IV-6A). This broad spectrum arose from the adduct of the catecholate monoanion, Fe(salen)DBCH (type I).* These changes could be observed for the solution prepared aerobically.

When more than twofold excess of *t*-BuOK was added to the Fe(salen)Cl:$DBCH_2$ 1:1 solution, the intensity of the chelated catecholate complex decreased extremely and the 3,5-di-*tert*-butyl-*o*-

* It was verified by measuring the Fe(salen)DBCH generating by another method (see Discussion).

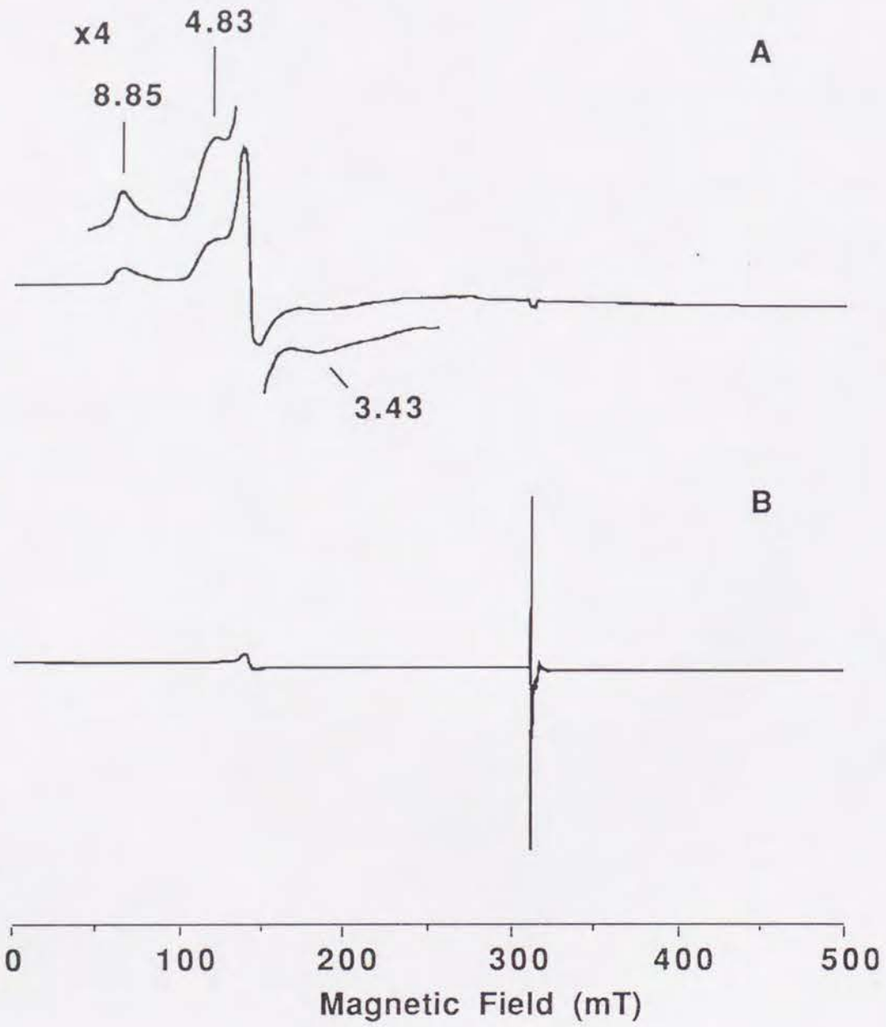

Figure IV-6. EPR spectra of (A) $[Fe(salen)DBC]^-$ and (B) $[Fe(salen)DBSQ]^-$ in MeOH at 4.2 K. Both samples were prepared anaerobically.

semiquinone (DBSQ) radical at g=2.004 was observed (Figure IV-6B). A similar result could be obtained from the sample prepared anaerobically. These observations indicate the following electron-transfer process:

$$[Fe(III)(salen)DBC]^- \longrightarrow Fe(II)(salen) + DBSQ^- \qquad (IV\text{-}1)$$

Figure IV-7 shows the time-course of the EPR and visible absorption spectra. The dashed line in each figure was obtained soon after the addition of *t*-BuOK (Fe:$DBCH_2$:*t*-BuOK=1:1:1.5). The EPR spectra with E/D=0.19 and the absorption spectra gave their maxima after several minutes and then decreased. Solid lines in each figure show changes after each gave their maxima. These spectral changes indicate that the species with E/D=0.19 corresponds to the one with λ_{max}=620 nm assigned as $[Fe(salen)DBC]^-$,[49] where the coordination mode of catecholate is bidentate (type II). There was no time-dependence with the sample prepared anaerobically.

The reaction time of the Fe(salen)Cl system is ca. 2—3 hours. The intermediate of type III structure, which is observed in the FeNTA system and gives the great influence on the reaction time, cannot be observed since the iron was reduced to ferrous state in such a structure.[48]

Fe(sal-L-aa)Cl System.

Fe(sal-L-aa)Cl did not react with $DBCH_2$ without alkaline reagents, but the addition of *t*-BuOK gave the catecholate complexes, as was the case of salen complex. Different kinds of catecholate intermediates were generated depending on the amount of the added *t*-BuOK, as was reported by Casella et al.[6] Figure IV-8 shows, for example, the absorption spectra of Fe(sal-L-val)–catecholate complexes. When *t*-BuOK was added to Fe(sal-L-val)Cl and $DBCH_2$ to give the molar ratio Fe:$DBCH_2$:*t*-BuOK=1:1:1, Fe(sal-L-val)DBCH was generated (solid line). The transition in the 400—500 nm region is assigned to phenolate to iron(III) LMCT band.[49a] When 2 equiv. of *t*-BuOK was added to the Fe(sal-L-val)Cl and $DBCH_2$ 1:1 solution, $[Fe(sal\text{-}L\text{-}val)DBC]^-$ (type II) was generated and the absorption around

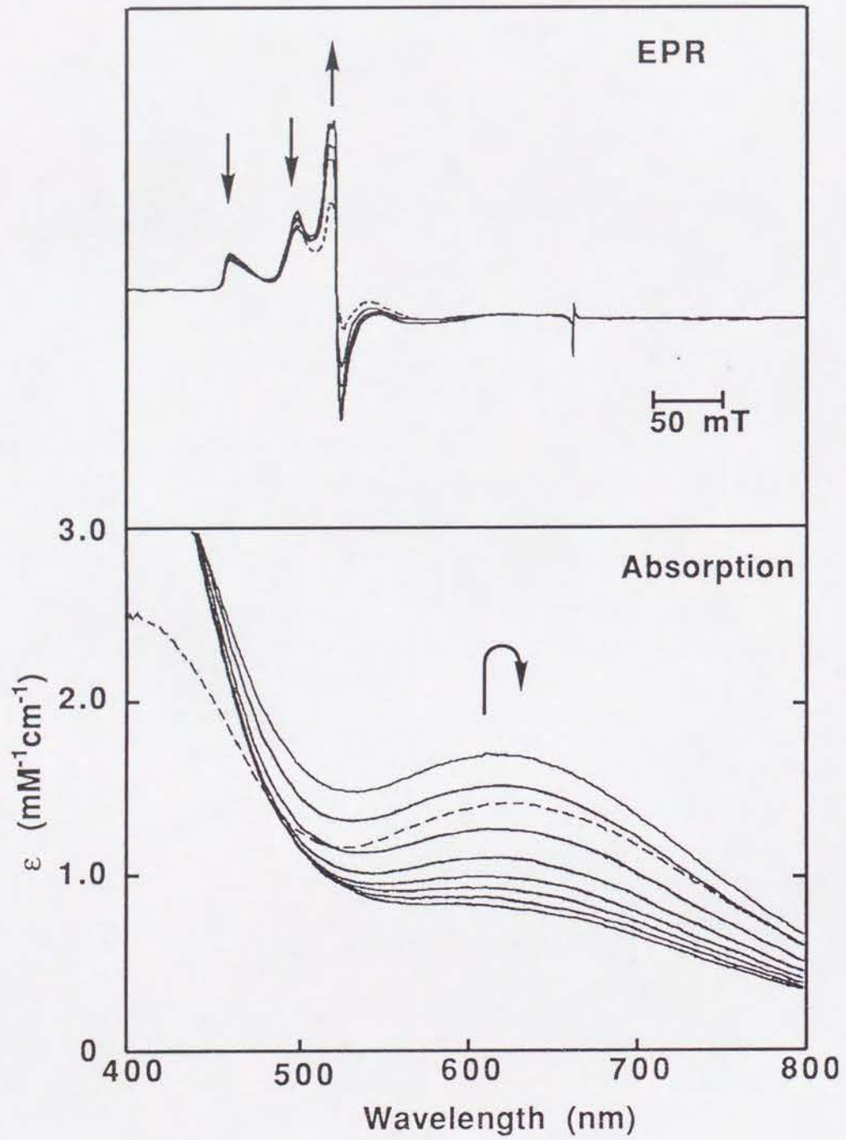

Figure IV-7. Time-dependent spectral changes of EPR (top) and visible absorption (bottom) accompanying *t*-BuOK addition (Fe:$DBCH_2$:*t*-BuOK=1:1:1.5). Dashed line in each figure is obtained immediately after addition of *t*-BuOK. Succesive scans (solid lines) begin 10 min. after *t*-BuOK addition and are 10 min (EPR) and 20 min (visible) apart, respectively.

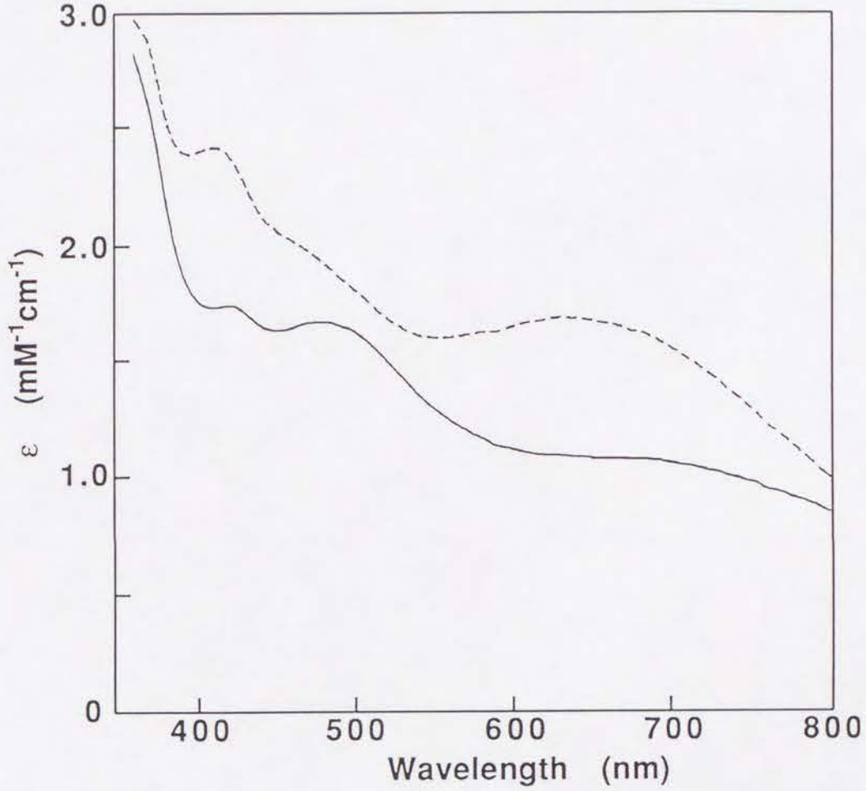

Figure IV-8. Visible spectra of Fe(sal-L-val)DBCH (solid line) and $[Fe(sal\text{-}L\text{-}val)DBC]^-$ (dashed line). Spectra were obtained anaerobically in MeOH solution.

620 nm (dashed line), assigned to catecholate to iron(III) LMCT band, appeared.

EPR spectra of Fe(sal-L-aa)Cl with *t*-BuOK are typical ones for non-heme iron complexes (E/D ~1/3) with peaks at g=9.6 and 4.3 in spite of the difference of the ligand type. Figure IV-9A shows the EPR spectrum of Fe(sal-L-val)DBCH. The same sample was used in the EPR and optical measurements. The spectrum shows two species with main E/D=0.32 (~80%) and minor E/D=0.13 (~20%). Other three sal-L-aa complexes showed similar spectra in spite of the difference, especially for histidine complex (type **B**), of the ligand structure (Table IV-3).

EPR spectra of four $[Fe(sal\text{-}L\text{-}aa)DBC]^-$ showed similar features to Fe(sal-L-aa)DBCH. However, additional smaller features arising from a trace amount of the chelated catecholate complex (E/D~0.20) were observed. Main features correspond to the adducts with the catecholate monoanion ($DBCH^-$; type I) and minor features to the adducts with the dianion (DBC^{2-}; type III). The generation of the catecholate dianion species is also supported by the broad features of 600—700 nm, assigned to catecholate to iron(III) LMCT band, in the absorption spectra (Figure IV-8 solid line). Although the absorption spectra of Fe(sal-L-aa)DBCH and $[Fe(sal\text{-}L\text{-}aa)DBC]^-$ are different from each other, EPR spectra of both are alike. These observations indicate that the both catecholate complexes have a similar iron environment. Taken together with the optical data, the coordination mode of the DBC^{2-} in minor species should be in a monodentate fashion (type III, *vide infra*).

The time-courses of EPR and optical spectra for Fe(sal-L-val)DBCH are shown in Figures. IV-9 (EPR) and 10 (optical). As the reaction with O_2 proceeded, the adducts of catecholate dianion (type III; E/D~0.13) gradually decreased and the uncomplexed $[Fe(sal\text{-}L\text{-}val)]^+$ increased (Figure 9B,C). No other species could be detected, but sometimes semiquinone radical could be observed (Figure 9). Since there was no apparent evidence for the ferric ion to be reduced in EPR spectra and the signal of the semiquinone radical could not be always detected, the iron ion in this system remained in the ferric oxidation state. Absorption spectra measured simultaneously show an

Table IV-3. EPR and Optical Data for Fe(sal-L-aa)-catecholate Complexes

complex	g values	E/D (±0.01)	λ_{max} (nm)
Fe(sal-L-ala)DBCH	4.44,4.25,4.11[a)]	0.30	400,466[b)]
$[Fe(sal\text{-}L\text{-}ala)DBC]^-$	8.16,5.55	0.11	400,625
Fe(sal-L-val)DBCH	4.46,4.24,4.10[a)]	0.30	417,473[b)]
$[Fe(sal\text{-}L\text{-}val)DBC]^-$	8.33,5.26	0.13	409,625
Fe(sal-L-phe)DBCH	4.52,4.20,3.96[a)]	0.29	414,472[b)]
$[Fe(sal\text{-}L\text{-}phe)DBC]^-$	8.85,5.37	0.16	400,628
Fe(sal-L-his)DBCH	4.37,4.25,4.14[a)]	0.31	417,470[b)]
$[Fe(sal\text{-}L\text{-}his)DBC]^-$	8.06,5.60	0.11	407,645

a) The g value of low field resonance (g~9.5) could not obtained due to the broad feature of the species with E/D ~0.13. b) The shoulder observed in 600—700 nm region is not shown.

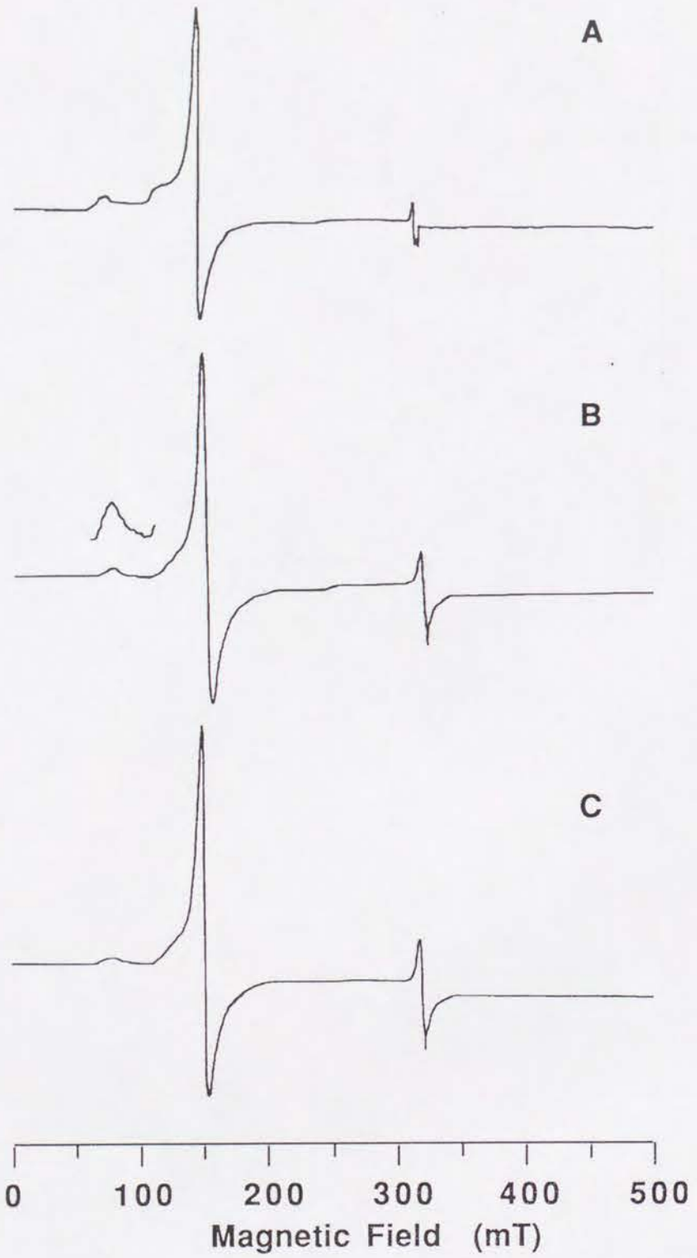

Figure IV-9 Progress of reaction of Fe(sal-L-val)DBCH in MeOH with O_2 as monitored by EPR spectroscopy. Spectra were obtained at 0, 20, and 40 min.

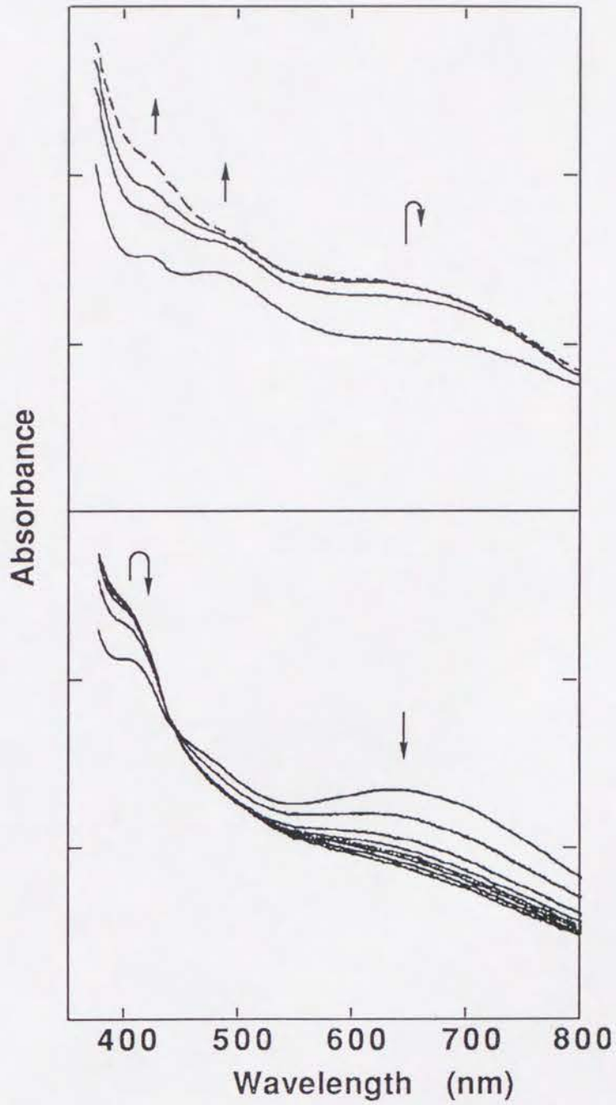

Figure IV- 10. Time-course of visible spectra of Fe(sal-L-val)DBCH (top) and $[Fe(sal\text{-}L\text{-}val)DBC]^-$ (bottom) in MeOH. *Top* : Spectral changes from Fe(sal-L-val)DBCH type to $[Fe(sal\text{-}L\text{-}val)DBC]^-$ type (dashed line) are shown. Successive scans are 10 min apart. *Bottom* : Decays of DBC complex are shown. Successive scans are 5 min apart.

interesting behavior (Figure IV-10 top). First, the Fe(sal-L-val)DBCH type absorption (solid line) was observed immediately after the addition of 1 equiv. of *t*-BuOK. As the reaction with O_2 proceeded, it shifted to the [Fe(sal-L-val)DBC]$^-$ type (dashed line), and then decreased gradually (not shown for clarity). These spectral changes clearly showed that the deprotonation from the catecholate monoanion did not affect the iron environment. Thus the minor species with E/D=0.13 should be the adducts of catecholate dianion in a monodentate fashion (type III). When 2 equiv. of *t*-BuOK was added to the reaction mixture, the [Fe(sal-L-val)DBC]$^-$ type absorption could be observed immediately and then decreased (Figure IV-10 bottom). No time-dependence in EPR and absorption spectra could be observed with samples prepared anaerobically.

The reaction time of the Fe(sal-L-aa)DBCH is ca. 1 hour. On the other hand, the reaction time of the [Fe(sal-L-aa)DBC]$^-$ is 20—30 min. This difference is due to the deprotonation process of the Fe(sal-L-aa)DBCH. In any case, Fe(sal-L-aa)Cl reacts with $DBCH_2$ and O_2 faster than FeNTA and Fe(salen)Cl.

Electrochemical Studies.

Complexes used in this study were also investigated electrochemically (Table IV-4). All the complexes except FeNTA show a redox process associated with the Fe(III)/Fe(II) couple, which ranges from –93 to –134 mV. For FeNTA, the redox process could not be observed due to lack of solubility to Me_2SO. In general, the redox

Table IV-4. Electrochemical Data for the Model Complexes

complex	E°' (mV)
FeNTA	—a)
Fe(salen)Cl	–100
Fe(sal-L-ala)Cl	–122
Fe(sal-L-val)Cl	–134
Fe(sal-L-phe)Cl	–109
Fe(sal-L-his)Cl	–93

a) FeNTA was not dissolved in Me_2SO.

potential shifts to more negative values as the electron donating alkyl group in the amino acid becomes large. Moreover, the redox potential shifts to positive values if the ligand has another pπ orbital in addition to the phenolate moiety of salicylaldehyde. From the results of EPR, only salen complex was shown to be reduced to ferrous state. With respect to the facility with reduction, however, the electrochemical data show no specialty of salen complex.

Oxygenation Studies.

We have investigated products obtained in the oxygenation of $DBCH_2$ (10 equiv.) in the presence of *t*-BuOK (10 equiv.), and Fe(sal-L-val)Cl (1 equiv.) in MeOH (10 mL) under atmospheric pressure of oxygen. Only $DBCH_2$ was used as a substrate because the *tert*-butyl groups minimize the side reactions and facilitate the product analysis. The main products isolated by silica gel chromatography were compounds **1**, **2**, and **3** (Scheme IV-5). Their structures are determined by ^1H NMR . The ^{13}C NMR spectral data of the products are also consistent with the structures. These products are derived from a muconic anhydride, 2,4-di-*tert*-butyl-2,4-hexadienedioic anhydride intermediate (**4**), produced by the intradiol dioxygenolysis of the substrate.

Since the preparative reaction was carried out in aqueous MeOH, the same medium as that in the EPR and optical measurements, compound **4** itself could not be isolated, because **4** is susceptible to nucleophiles such as H_2O and MeOH. If H_2O attacks on the less hindered carbonyl in **4** followed by an intramolecular conjugate addition, then 2,4-di-*tert*-butyl-4-(carboxymethyl)-2-buten-4-olide (**5**) is obtained. Compound **1** is derived from further oxidation of **5**. The ^1H NMR spectrum of a fraction including **1** shows the presence of a small amount of **5**. This would suggest that compound **1** may result from further oxidation of **5** under the condition. However, Funabiki et al.[11] reported that **1** could be a primary product resulting from an extradiol type oxygenation in the $FeCl_3$/bpy/py system. On the other hand, if MeOH attacks, methyl esters are produced. Whether **2** or **3** is yielded depends on the position where the cyclization occurs. In

Scheme IV-5.

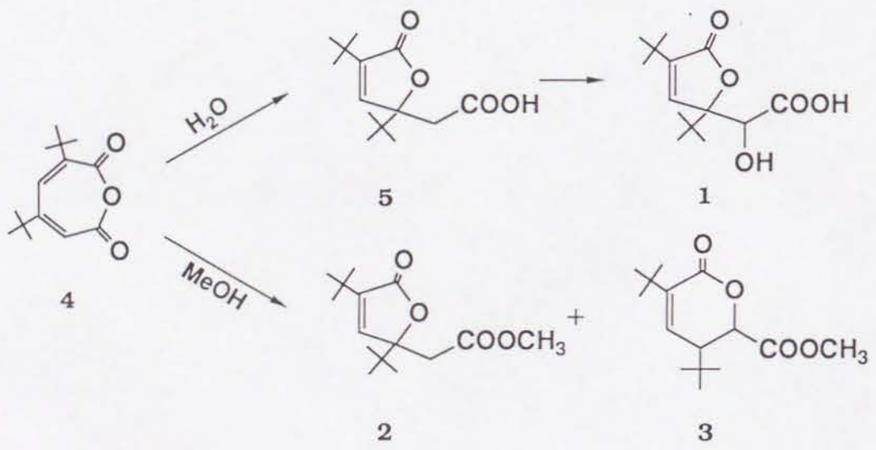

4 **5** **1** **2** **3**

Scheme IV-5.

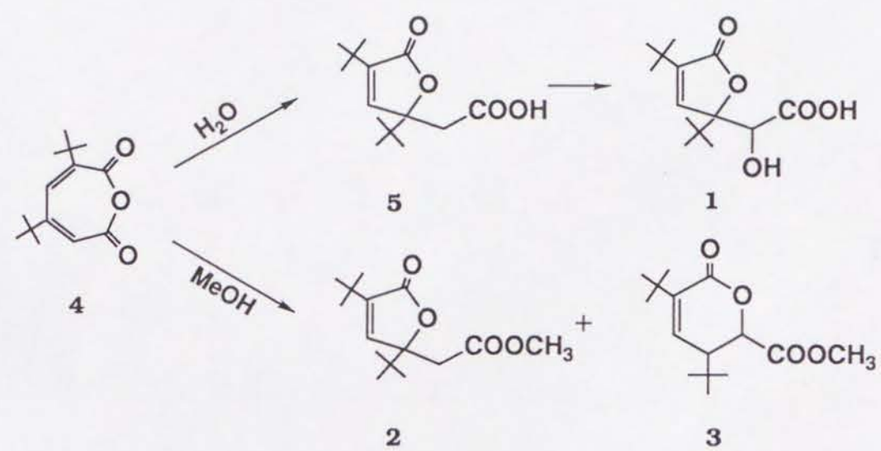

4 **5** **1** **2** **3**

anyway, the immediate product is **4**. Besides the main products, **5**, a trace amount of quinone and some unknown products were also yielded. No unreacted $DBCH_2$ were isolated. Although the exact yield of the products due to dioxygenolysis of the aromatic ring could not be calculated because of the polymerization of the products, the total yield of **1**, **2**, and **3** is not less than 80 % of the starting $DBCH_2$. Base can catalyze the oxygenation of $DBCH_2$.[51] However, since only 1 equiv. of *t*-BuOK relative to $DBCH_2$ was added to the reaction mixture, the solution was nearly neutral during the reaction. Moreover, the product composition observed without the iron complex is different from that with the iron complex. Taken together with the EPR results, these observations indicate that Fe(sal-L-val)Cl serves as a highly specific catalyst for the ring cleavage of catechols not involving the redox process of iron ion.

2,4-Di-*tert*-butyl-4-(1-carboxy-1-hydroxymethyl)-2-buten-4-olide (**1**): ^1H NMR ($CDCl_3$) δ 1.06 (s, 9H), 1.21 (s, 9H), 4.70 (s, 1H), 7.12 (s, 1H); ^{13}C NMR δ 25.9 (q), 28.0 (q), 31.6 (s), 38.0 (s), 77.1 (s), 89.9 (s), 143.2 (s), 145.2 (s), 171.8 (s), 174.7 (s)

2,4-Di-*tert*-butyl-4-(methoxycarboxylmethyl)-2-buten-4-olide (**2**): ^1H NMR ($CDCl_3$) δ 0.95 (s, 9H), 1.22 (s, 9H), 2.79 (d, *J*=14.1 Hz, 1H), 2.93 (d, *J*=14.1 Hz, 1H), 3.57 (s, 3H), 6.96 (s, 1H)

2,4-Di-*tert*-butyl-5-methoxycarboxyl)-2-penten-5-olide (**3**): ^1H NMR ($CDCl_3$) δ 1.04 (s, 9H), 1.19 (s, 9H), 3.16 (d, *J*=7.83 Hz, 1H), 3.70 (s, 3H), 4.69 (d, *J*=7.83 Hz, 1H), 7.09 (s, 1H); ^{13}C NMR ($CDCl_3$) δ 25.8 (q), 28.1 (q), 31.7 (s), 38.0 (s), 53.1 (s), 73.0 (s), 89.3 (s), 139.7 (s), 144.4 (s), 170.7 (s), 173.2 (s)

IV-4. Discussion.

The Structures of Intermediate Catecholate Complexes.

We have investigated the CTD model reactions utilizing FeNTA, Fe(salen)Cl, and Fe(sal-L-aa)Cl as catalyst. EPR parameters and reaction times of typical catecholate complexes are shown in Table IV-5. From a perusal of the Tables IV-1, IV-3, and IV-5, it is clear that

Table IV-5. Relation between EPR Parameters and Reaction Time

complex	*E/D*	ratio (%)	Reaction Time
$[Fe(NTA)DBC]^{2-}$	0.20	~95	7 days
	0.13	~5	
$[Fe(NTA)cat]^{2-}$	0.20	~100	10 days
Fe(salen)DBCH	0.30	~50	2 ~ 3 hours
$[Fe(salen)DBC]^{-}$	0.19	~50	
Fe(sal-L-val)DBCH	0.30	~80	30 ~ 60 min
$[Fe(sal\text{-}L\text{-}val)DBC]^{-}$	0.13	~20	

the values of *E/D*, a measure of the departure of the electronic environment of the iron from axial symmetry, concentrate on the three distinct ranges, ~0.30, ~0.20, ~0.12 (Figure IV-11). Furthermore, these three correspond to the modes of the catecholate coordination, i.e. monoanionic catecholate (~0.30; type I), chelated catecholate (~0.20; type II), and monodentate dianionic catecholate (~0.12; type III), respectively, as described in the results section. For the reaction of FeNTA with $DBCH_2$, type II is observed as a major intermediate along with a trace amount of type III, only type II with other catecholates. For Fe(salen)Cl, they are comparable amount of type I and type II, and ferrous-semiquinone species. For Fe(sal-L-aa)Cl, major type I and minor type III are observed.

Among three types of catecholate coordination modes, type I and II were confirmed by X-ray crystallography. The crystal of Fe(saloph)catH† shows square-pyramidal geometry with monoanionic monodentate catecholate (type I).[52] On the other hand, K[Fe(salen)cat][53] and $(dabcoH)_2[Fe(NTA)DBC]$[4] are six-coordinate high-spin ferric complexes with chelated catecholates (type II). We have assigned the structures of type I, II, and III for the species with *E/D*~0.30, ~0.20, and ~0.12, respectively. These assignments are also supported by the following observations. The EPR spectrum of $(dabcoH)_2[Fe(NTA)DBC]$ in DMF/Me_2SO/toluene frozen glass[50]

† : Abbreviations: saloph, *N,N'*-(1,2-phenylene)bis(salicylidenimine) dianion; dabco, 1,4-diaza-bicyclo[2,2,2]octane

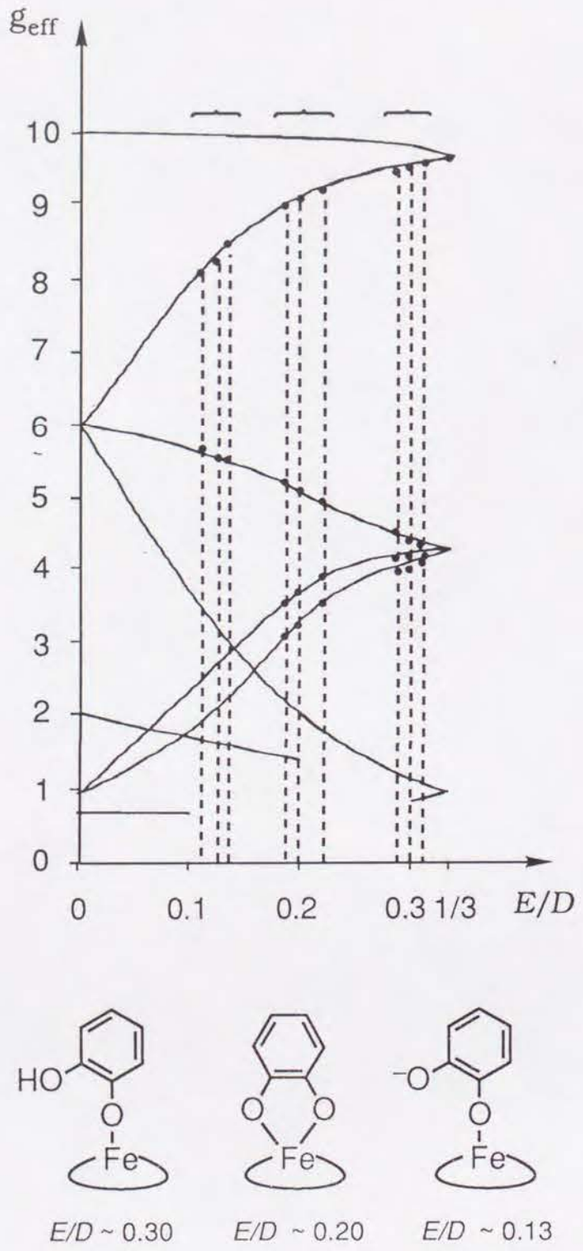

Figure IV-11. Plots of the observed g values as a function of E/D in CTD model systems.

shows similar features to our spectrum of $[Fe(NTA)DBC]^{2-}$ generated from $Fe(NTA)\cdot 2H_2O$ with $DBCH_2$ in a DMF/borate buffer; thus, the species with E/D~0.20 certainly corresponds to the bidentate catecholate complex. Fe(salen)DBCH, generated from ligand exchange of Fe(salen)OAc (OAc: acetate) with excess $DBCH_2$[49], exhibits a broad features at g=4.3 (E/D~0.30; not shown). Unfortunately, there is no method for generating the species of type III structure certainly. However, considering the EPR change from Fe(sal-L-aa)DBCH to $[Fe(sal\text{-}L\text{-}aa)DBC]^-$, it is most likely that the species with E/D~0.12 will have the type III structure. Such structure is expected to be stabilized by polar solvents such as DMF and MeOH used in this study. From the CD studies,[6] it is suggested that the complexes with type **A** ligand of sal-L-aa can provide two coordination sites (one axial and one equatorial) that can be occupied by an additional ligand and that the catecholate binds to the iron ion in a bidentate mode. Our EPR results, however, indicate the monodentate binding of catecholate dianion.

EPR spectra of enzyme-substrate and enzyme-inhibitor complexes have been reported. For example, the parameters are E/D=0.02 and 0.12 for PCD-PCA (substrate) complex,[42] E/D=0.02 and 0.33 for PCD-HPCA (slow substrate) complex,[54] and E/D=0.32 and 0.24 for PCD-4-hydroxybenzoic acid (inhibitor) complex.[54] Orville and Lipscomb[54] proposed a monodentate catecholate structure for the species with E/D=0.02. The E/D values of enzymes and model complexes cannot be compared indiscriminately because of the difference of the ligand flexibility to the exogenous catecholate or O_2 binding. In fact, PCD-substrate complex gives new species when O_2 is introduced,[42] while the model complexes give no new one. However, there is the tendency that plural species are generated in both cases. In the cases of our model systems, it is confirmed by EPR that there are three types of intermediates, monodentate monoanionic catecholate complex (type I, E/D~0.30), bidentate catecholate one (type II), and monodentate monoanionic catecholate one (type III), in the reaction mixtures.

Mechanistic Implications.

These structural data taken together with the reaction time afford interesting insights into the mechanism of the CTD-like reaction. The more stable chelated catecholate complex results in the slower reaction with O_2. Conversely, the reaction proceeds fast as the ratio of the type III intermediate becomes high. These relation indicate that the chelated catecholate intermediate (type II) is the inactive species, and that monodentate dianionic catecholate intermediate (type III) is the one reactive toward O_2. Que and co-workers[4,45,47] reported the correlation between the rate of the reaction and the Lewis acidity of the ferric center. Our results demonstrate that the structure of the dominant intermediate also affects the reaction rate of oxygenation of catechols.

On the basis of our results, we propose a mechanism for the CTD-like reaction catalyzed by three model complexes. For FeNTA system (Scheme IV-6), a substrate binds to the ferric center in a bidentate fashion. Some of these chelated complexes dissociate one catecholate oxygen from the metal center, and this monodentate catecholate complex then react with O_2 to yield an intermediate peroxide complex, which then decomposes to form the muconic anhydride. For Fe(salen)Cl system (Scheme IV-7), a substrate binds to the ferric center in a bidentate or a monodentate fashion. Since the type I intermediate reacts with O_2 to form a DBSQ,[48] a reactant of O_2 to produce the muconic anhydride is probably the Fe(II)(salen)DBSQ$^{\bullet}$. For Fe(sal-L-aa)Cl system (Scheme IV-8), the substrate $DBCH_2$ first coordinates to the ferric ion in a monodentate fashion as $DBCH^-$ form, and then loses another proton. Since each sample prepared aerobically or anaerobically gives similar EPR spectrum until this stage of the reaction, the type III intermediate may be generated independent of the presence or absence of oxygen. The carbanion resulting from the tautomerization of the type III intermediate reacts with O_2 to produce a peroxide complex, which then decomposes to compound **4**. The deprotonation process of the iron-bound catecholate is clearly demonstrated by the changes in the absorption spectra (Figure IV-10 top). In this process, the ferric center seems to serve as a promoter of deprotonation of catecholate

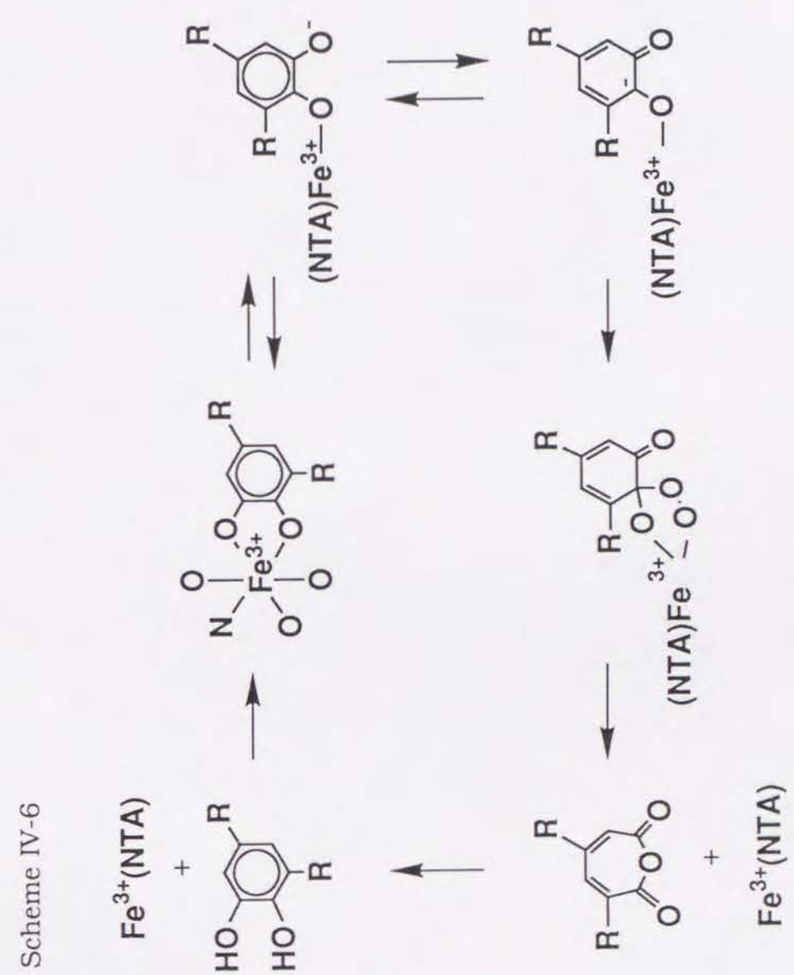

Scheme IV-6

Scheme IV-7

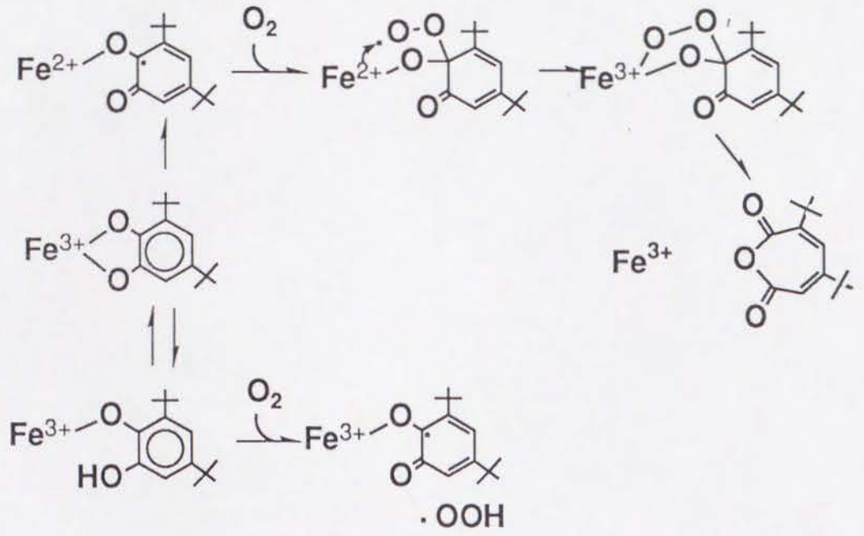

Scheme IV-8

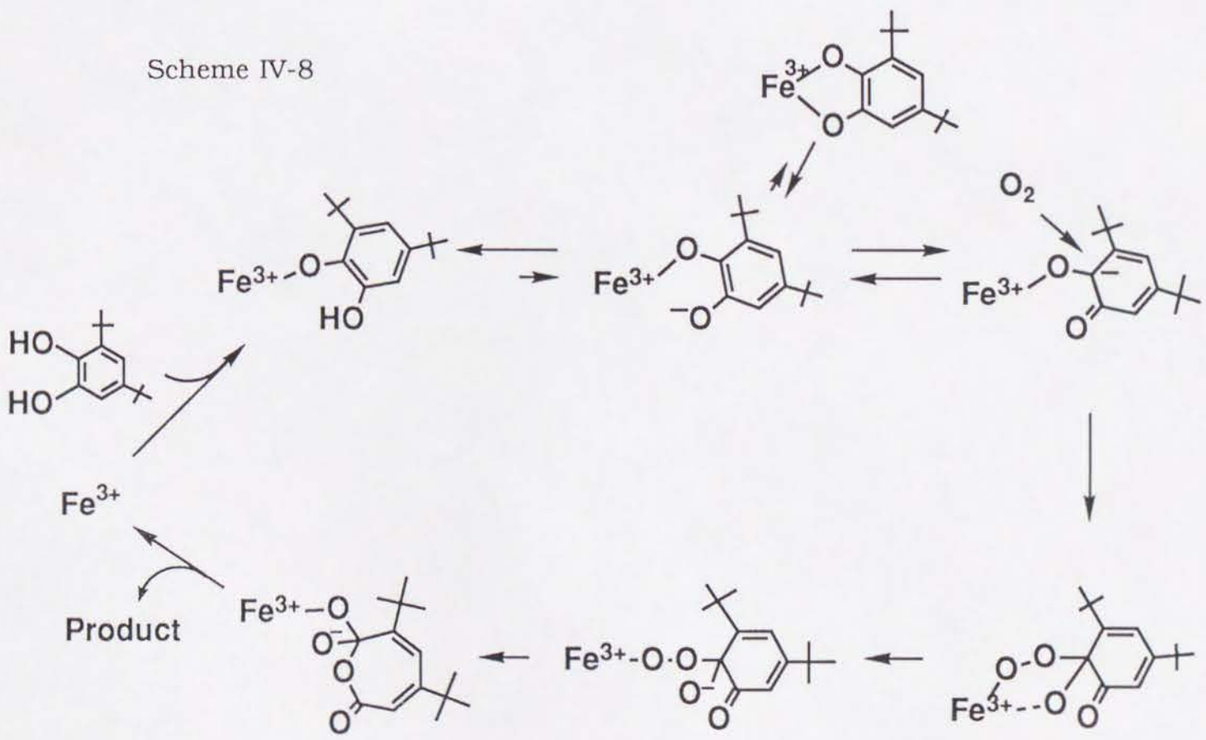

monoanion, $DBCH^-$. It is conceivable that this function is attributed to the Lewis acidity of the ferric center. However, such apparent spectral changes could not be observed when Fe(sal-L-aa)DBCH was prepared anaerobically; therefore, dioxygen may be participated in this process. The peroxide complex is indispensable for the oxygenation reaction.[55,56] Such a peroxide complex was crystallized in the case of the oxygenation of 2,4,6-tri-*tert*-butylphenol by Co(salpr)†[56b]. Recently, the crystal structure of Ir(III)-catecholate peroxide complex was reported as a CTD model.[57] In the oxygenation of catechols, the Lewis acidity of the end of the peroxide bound to the root of a hydroxyl of a catechol affects the mode of oxygenation. Strong Lewis acidity leads the intradiol cleavage products, on the other hand, weak Lewis acidity does the extradiol ones.[58] This is consistent with the results reported by Que et al. that the yield of the intradiol products increased as the Lewis acidity of the metal center increased.[4] Thus, at this stage of the reaction, Fe(III) is favorable.

The above-mentioned mechanism is similar to that proposed previously[4] except for the intervention of the chelated catecholate complex during the catalytic cycle. This proposed mechanism involving the chelated catecholate intermediate is similar to that of FeNTA system we proposed (Scheme IV-6).[48] The virtue of the Fe(sal-L-aa)Cl system is that there is little, if any, amount of the chelated catecholate complex; thus, the monodentate species are predominant. The monodentate coordination of the catecholate facilitates a keto-enol-like tautomerization of the catecholate to provide an available coordination site for the formation of the peroxide complex. For the FeNTA and Fe(salen)Cl systems where the chelated catecholate intermediate is the dominant species, the dissociation of one catecholate oxygen from the ferric ion is required to form the peroxide complex. Consequently, the reaction of $[Fe(sal\text{-}L\text{-}aa)DBC]^-$ with O_2 would proceed faster than that of other two substrate complexes.

Taken the intensity changes in the EPR spectra and the observations of organic radicals into consideration, the iron center retains the ferric state throughout the reaction utilizing the FeNTA

† Abbriviation: salpr, *N,N'*-bis(salicylidene)-1,3-propanediamine

and the Fe(sal-L-aa)Cl systems, whereas with the Fe(salen)Cl system the ferric center is reduced to the ferrous state during the reaction. Presumably, O_2 reacts with the ferric-catecholate carbanion species in the former case, while with on the ferrous-semiquinonate species in the latter case. In the Fe(salen)Cl system, however, the type III intermediate, which is probably the reactive species toward O_2 in this system, could not be observed because the reduction of the ferric ion may take place during the structural change from the type II to the type III (Scheme IV-7).[48] The reduction of the ferric center unique to the salen complex may be attributed to the effect of the ligand distortion. The cyclic voltammograms of all the model complexes used in this study show the redox couple (Fe(III)/Fe(II)) near −110 mV (Table IV-4). Since salen is a planar ligand having two phenolate $p\pi$ orbitals overlapped directly with the $d\pi$ orbitals in the ferric ion, catecholate coordination in a bidentate mode is expected to distort the ligand and to affect the redox potential of iron in $[Fe(III)(salen)]^+$; indeed, the crystal of $[Fe(salen)cat]^-$ exhibits the distorted octahedral structure with the distorted salen ligand.[53]

Recently, Funabiki et al.[59] and Que et al.[47] reported that the bound catecholate had a strong radical character and proposed the Fe(II)-semiquinone intermediate as a reactive species toward dioxygen. Both groups deduced their conclusion from the NMR downfield shifts of the catecholate ligand. Funabiki et al. also reported that the equivalents of Fe(II) and Fe(III) were observed in the Mössbauer spectrum on the $FeCl_3$/bpy/py–$DBCH_2$ system.[46b] On the contrary, Mössbauer[38-40] and EPR[38-40,42,54] studies of enzyme-substrate complexes indicate the Fe(III)-catecholate species. Our results obtained from the present model studies suggest that both are probable candidates for a reactive species toward O_2, i.e. the Fe(III)-catecholate species for FeNTA and Fe(sal-L-aa)Cl, and the Fe(II)-semiquinonate species for Fe(salen)Cl. Even in the FeNTA and the Fe(sal-L-aa)Cl system, it is conceivable that only a few amounts of Fe(II)-semiquinonate species are generated, because it is difficult to judge such a thing from EPR or other spectroscopies. However, taken the resultant products into consideration, Fe(III)-catecholate species is more likely. FeNTA[4,43] and Fe(sal-L-aa)Cl give a ca. 80 % yield of the

ring cleavage products, while Fe(salen)Cl, where the Fe(II)-semiquinonate is probably a reactive species toward O_2, gives a ca. 30 % yield.[4] Even being subtracted the effect of the side reaction of Fe(salen)DBCH with O_2 (Scheme IV-7),[49a] the salen complex would be a less efficient catalyst than other two complexes. Further information about the products yields by ferrous species was reported by Funabiki et al.[44] In the $FeCl_3$/bpy/py system, where the presence of equimolar amounts of Fe(II) and Fe(III) are observed, the main product (50~70 %) is 3,5-di-*tert*-butyl-1,2-benzoquinone and the total yields of the ring cleavage products is less than 50 %. An interesting relation is also pointed out by Cox and Que:[45] the relation which stronger semiquinone character of iron-bound catecholate brings less specificity for intradiol cleavage. Although all the factors of these less specificity toward the ring cleavage products could not be ascribed to the Fe(II)-semiquinone species, there seems some relations between the yields of the ring cleavage products and the Fe(II)-semiquinone intermediate. Although our EPR and optical results, of course, cannot definitely exclude the possibility that the Fe(III)-catecholate species has the Fe(II)-semiquinone character, we prefer the Fe(III)-catecholate intermediate from these considerations.

Conclusion.

We have investigated the structures of the intermediates appeared in the CTD model systems. There are three types of intermediates which have different coordination modes of the catecholate. Among these three, the Fe(III)-monodentate dianionic catecholate (type III) is most probable as the direct reactant with O_2. In enzyme systems, the participation of the chelated catecholate in the catalytic cycle has been proposed by EPR[54] and EXAFS[60] studies. For FeNTA and Fe(salen)Cl system, the chelated catecholate intermediates could be detected. In the case of Fe(sal-L-aa)Cl, however, the chelated catecholate species (type II) could not be detected. It is a novel point of this system. In order to elucidate the reaction mechanism of the Fe(sal-L-aa)Cl system, further systematic investigations are now under way.

In the CTD model systems, the iron ion would serve two functions. First, the ferric center would serve to coordinate and activate the substrate by promoting the loss of both catecholate protons and delocalizing unpaired spin density into the catechol ring. This is due to the Lewis acidity of the ferric ion. Second, relating with the first function, the ferric center serves to promote the decomposition of the peroxide complex to yield the muconic anhydride. It is also suggested that the ligand nature affects the redox potential of the iron ion.

V. Correlation between the EPR Parameters and the Coordination Environments of Non-Heme Ferric Complexes.

In the preceding two chapters, we investigate the structures of intermediates generated in the model reactions of non-heme iron enzymes. Through a careful scrutiny of the data obtained, we found an interesting relation between the structures of intermediates and the EPR parameters. Using this relation with care, it is possible to obtain useful information in the structural studies of the non-heme iron complexes, and the non-heme iron enzymes.

V-1. Survey of the EPR spectrum of Non-Heme and Heme Ferric Enzymes and Complexes.

Before discussing the correlation, we would like to survey the EPR spectra of non-heme ferric ions and to reveal the problems of them. Further, we deal with the application of EPR to the ferric low-spin heme enzymes. The electronic structure of ferric low-spin heme enzyme is closely related to the EPR parameters (g value), so that the structural information about the heme enzyme is easily obtained from the spectra.

The Problems of the EPR Spectra of the High-Spin Ferric Non-Heme Complexes.

The typical EPR spectrum of the high-spin non-heme ferric ion exhibits one sharp signal at g=4.3 (See for example, Figure III-a, or Figure IV-5 left D). This has been interpreted in terms of a spin Hamiltonian (eq.II-1) for S=5/2 since Castner et al.[61] succeeded in the explanation of its origin. Since then, a lot of theoretical studies have been made to explain the observed g values of non-heme ferric ions under various environments.[62-68] Essentially, as described in the section II-3, the observed g values of non-heme ferric ions only

depend upon the E/D (See Figure II-1) due to the three Kramers doublets at zero field. The fine structure parameters E (rhombicity) and D (zero field splitting) reflect the symmetry of the paramagnetic site as the ratio E/D. As pointed out by Blumberg,[69] all symmetries distinguishable in EPR by effective g values can be represented on the interval $0 \leq E/D \leq 1/3$. $E/D = 0$ corresponds to the axial symmetry, which shows g=6 and 2 resonances, and $E/D = 1/3$ to the rhombic symmetry, which shows g=4.3 resonance. Despite a variety of coordination environments, almost non-heme iron complexes in the solution and enzymes in their resting states show the EPR spectra at g=4.3 with $E/D \sim 1/3$. One of the most important problem to be solved is why they exhibits similar EPR spectra with $E/D=1/3$ (g=4.3) regardless of the differences in the structures.

However, the EPR spectra change with the coordination of exogenous ligands to the ferric center. Typical examples are shown in Figures. III-3, IV-3, IV-6, and IV-9. What occurs to the ferric ion? Does the structural change affect the electronic structure of ferric ion? The answer to the second question is probably yes. If so, why the original complexes show similar EPR spectra with $E/D=1/3$? In the original complexes, the electronic structures of the ferric ions must differ with each other. What electronic structure does the ratio $E/D=1/3$ reflect? Like this, our discussion go around in circles.

Unfortunately, there have been no theory to answer these questions clearly. Furthermore, there have been little attempt to throw a light on these questions. The treatment by the angular overlap model (AOM)[70] is one of the most successful theoretical treatment. Fukui et al. investigated the relation between zero-field splittings and distortions along the normal coordinates in transition metal complexes.[71] Their AOM treatment reveals that Ev-type and T_2z-type distortions in an octahedral or a tetrahedral complex realize the electronic structure represented as $E/D=1/3$. However, there present non-heme iron enzymes which show the EPR spectra with $E/D=1/3$ but has other distortion types.

As described above, there still remain important problems of the non-heme iron complexes and enzymes. Consequently, we cannot derive the information about the coordination environment as well as

the one about the electronic structure from the EPR spectra. In the following section, we will survey the case of the heme enzymes and model complexes where the EPR is a strong tool to get the structural information.

Application of EPR to Low-Spin Ferric Heme Enzymes and Model Porphyrin Complexes.

In the case of heme enzymes and the model porphyrin complexes, circumstances are fairly different from those of non-heme system. Since heme enzymes as well as model porphyrin complexes have a common porphyrin ligand (four pyrrole nitrogen), the unknown ligands are only two axial ones. Moreover, the porphyrin is a strong planar ligand, so that the molecular z-axis can be easily determined. The information about the molecular axes is very useful to investigate their electronic structures. This advantage is marked in low-spin heme complexes.

In the studies of low-spin ferric hemoproteins and model complexes, EPR spectroscopy has been one of the most useful tools for characterizing them. This is largely due to the fact that the EPR parameters (g values) may be used to calculate the relative energies of the d orbitals d_{xy}, d_{xz}, and d_{yz}. Peisach and Blumberg developed a method of this analysis which allows the identity of the axial ligands to be assigned.[72,73] Since Griffith outlined first the theory used to calculate the d-orbital energies,[74,75] several workers elaborate the theory.[76-79] The salient features may be summarized as follows: Figure V-1 shows the electronic structure of low-spin Fe(III) in rhombically distorted system, where Δ is a tetragonal splitting parameter and V is a rhombic splitting parameter. Since the total spin of the low-spin ferriheme is S=1/2, the two wave functions (for α and β spin) are thus linear combinations of the three states with coefficients a (for d_{yz}), b (for d_{xz}), and c (for d_{xy}). When the axis system of Taylor is used,[78] it can be shown that

$$a=(g_x + g_y)/4K$$

$$b=(g_z - g_x)/4K$$

$$c=(g_y - g_x)/4K \qquad \text{(V-1)}$$

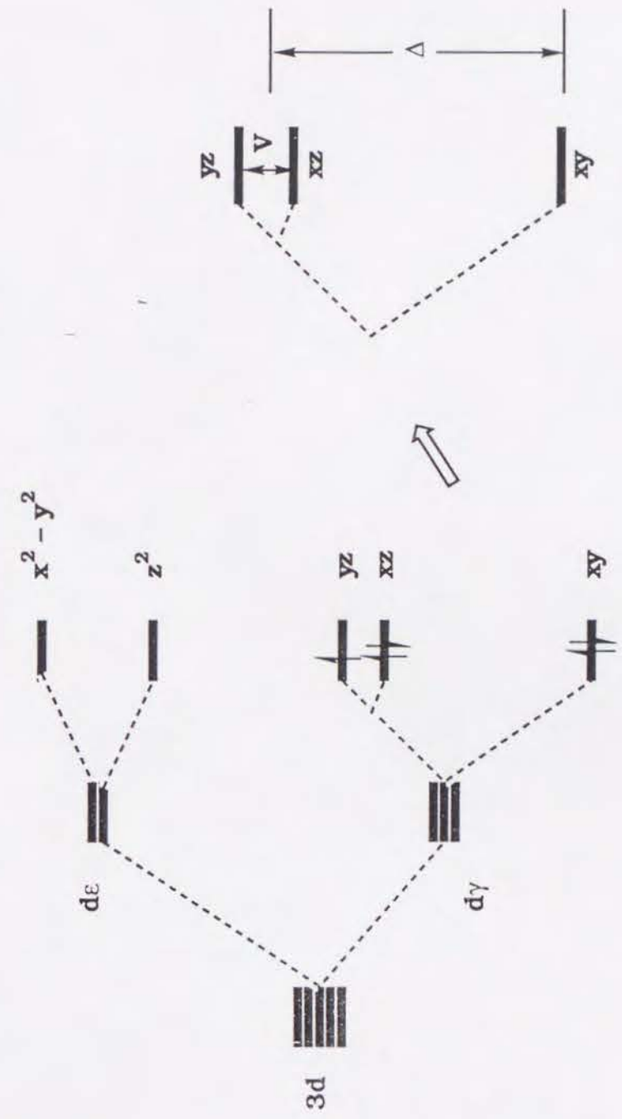

V: rhombic splitting

Δ: tetragonal splitting

Figure V-1. The electronic structure of low-spin ferric ion.

where $4K=[8(g_z+g_y-g_x)]^{1/2}$. From these quantities, a, b, and c, the relative energies of the three d orbitals of Figure V-1 can be determined. Further from these quantities, tetragonal (Δ/λ) and rhombic (V/λ) splitting parameters may be calculated:[80]

$$\frac{V}{\lambda} = E_{yz} - E_{xz} = \frac{g_x}{g_z + g_y} + \frac{g_y}{g_z - g_x} \qquad \text{(V-2)}$$

$$\frac{\Delta}{\lambda} = E_{xz} - E_{xy} - \frac{V}{2\lambda} = \frac{g_x}{g_z + g_y} + \frac{g_z}{g_y - g_x} - \frac{V}{2\lambda} \qquad \text{(V-3)}$$

Peisach and Blumberg first used such equations to determine the rhombicity (V/Δ), which is purely geometric factor, and tetragonality (Δ/λ), which is a measure of ligand donor strength, of various low-spin hemoproteins and model complexes, and have found that those known to have the same axial ligands fall into very small regions of the plot.[72,73] Five ligand combinations which is occurred naturally (P: -SH and $-OH^-$; O: $-OH^-$ and His; H: His and His (protein denatured; B: His and His; C: His and SR_2) have been outlined.[78]

By using eq.V-2 and V-3, and this relation known as 'Blumberg-Peisach plot', one can easily get the information not only about the electronic structure but also about the coordination environment of the ferric center from the observed g values.

V-2. An Attempt to Find the Correlation between the EPR Parameters and the Coordination Environments of Non-Heme Ferric Complexes

As discussed in the section V-1, there is a great difference between the heme iron and non-heme iron in the application of EPR. For the heme enzymes and the model complexes which have a common porphyrin ligand, their axial ligands can be deduced from the parameters tetragonality and rhombicity calculated from the observed g values as described in the precedent section. On the other hand, such a relation has not been reported in the cases of non-heme iron

enzymes and complexes. Therefore, it is expected to find a relation between the EPR parameters and the coordination environments of non-heme ferric enzymes and complexes.

In the course of our investigations of the reactions of non-heme ferric complexes with various substrates, we have found an interesting tendency of the EPR spectra. First, we investigated the structure of the peroxo intermediate formed in Fe(III)EDTA system in Chapter III. The end-on type peroxo complexes, Fe(III)EDTA-$^-$OOR (R=H, *n*-butyl, and *t*-butyl) show the EPR spectra with E/D~0.30, on the contrary, the side-on type peroxo complex, Fe(III)EDTA-O_2^{2-}, exhibits with E/D~0.20. Next, we investigated the structures of intermediate catecholate complexes in Chapter IV. In the CTD model systems, monoanionic monodentate catecholate complexes (type I in Scheme IV-4) show the EPR spectra with E/D~0.30, dianionic bidentate catecholate complexes (type II) with E/D~0.20, and dianionic monodentate catecholate complexes (type III) with E/D~0.12. Other examples are the Fe(III)-peroxide complexes of EDTA derivatives and the Fe(III)-phenolate complexes. The peroxide complexes of EDTA derivatives also exhibit similar behavior to EDTA itself.[44] Phenolate coordination to the non-heme ferric complexes used in these studies gives the EPR spectrum with E/D~0.30.

Our observations indicate a correlation between the E/D estimated from the observed g values and the number of exogenous oxyanion ligands, i.e. E/D ~0.30 for one exogenous oxyanion ligand, E/D ~0.20 for two exogenous ones both of which bind to the ferric center, and E/D ~0.12 for two exogenous ones one of which, however, is in the proximity of the ferric center but does not bind to it (type III conformation in CTD models). Unfortunately, this correlation cannot apply to other exogenous ligands such as nitrogen; indeed, pyridine or bipyridine coordination gives entirely different tendencies. When the exogenous nitrogen ligates to the iron center, the complex shows completely rhombic EPR spectra with E/D=1/3. This is explained qualitatively as follows. The D and E are ligand field parameters which include the effects of ligands electrostatically. Accordingly, it is natural that the influence given by an anionic oxygen should be different from that given by neutral nitrogen. It is also the case with

the number of exogenous oxyanion ligands. Probably the conformation corresponding to E/D~1/3 is most stable for the non-heme iron complexes in solution and for most of the non-heme iron enzymes in their resting state. When the exogenous oxyanion binds to the ferric center, the conformation of the original ligands would change to a new stable state. In this point, there will be a difference between complexes and enzymes due to the difference of the flexibility of the original ligands. In the complexes, the ligands are relatively labile, so that the conformation change should easily occur. On the other hand, as for the enzymes, the ligand are amino acid residues of polypeptide, so that the conformation change is less possible. As a consequence, the ligand field effect influenced by the coordination of the exogenous ligands may be different between the complexes and the enzymes. Accordingly this correlation found in the complex system will not necessarily apply to the enzyme systems.

Nevertheless, the plots of the reported g values against E/D suggest another interesting tendency (Figure V-2). From the Figure V-2, we can separate the non-heme iron enzymes and complexes into five or four (if δ includes ε) groups. Since there are a few non-heme iron enzymes whose active site structure is revealed, we cannot treat a relation in detail, but it should be noted that the only enzymes belong to the α group.

We have been attempting to give a theoretical explanation to the relation we found, but have not succeeded yet. However, we think it a clue to an exploration into the theoretical analysis and the more general correlation between the coordination environments of the non-heme iron ions and the EPR parameters.

Figure V-2. Plots of the observed g values of various non-heme iron complexes and enzymes as a function of E/D.

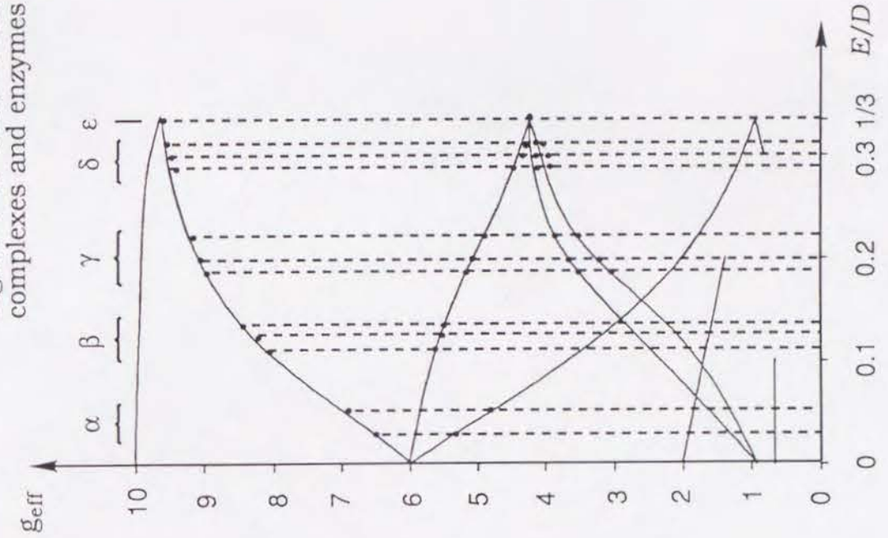

Summary

In the present thesis the author has attempted to elucidate the reaction mechanisms of superoxide dismutase and catechol dioxygenases by using model complexes. Fe(III)EDTA were used as a model for SOD and FeNTA, Fe(salen)Cl, and Fe(sal-L-his)Cl (aa: ala, val, phe, his) were used as models for CTD. In both cases, attempts were made to determine the structures of intermediates generated in the model reaction systems mainly by EPR spectroscopy. Furthermore, on the basis of the observations, the attempt to find a correlation between the EPR parameters and the coordination environments of the non-heme ferric complexes was also made.

In Chapter III, we succeeded in the determination of the structures of intermediates appeared in a SOD model system. In this model system, the side-on peroxo complex play a key role in the reaction. The presence of the monodentate hydroperoxy complex is first confirmed by this study. The ferrous superoxo complex is also detected. This is one of a rare example of the metal-bound superoxide radical. Especially, this is the second example of the iron-bound one as far as we know. The redox cycle formed by FeEDTA with superoxide and peroxide is also confirmed.

Chapter IV is devoted to determine the structures of the catecholate intermediates and to elucidate the reaction mechanism of the catechol dioxygenases by using three kinds of model complexes. Three types of catecholate intermediates are detected by EPR. In the FeNTA and the Fe(sal-L-aa)Cl system, our results obtained indicate that the Fe(III) intermediates are only present in the reaction mixtures. However, our results obtained in the Fe(salen)Cl system clearly demonstrate the generation of Fe(II)-semiquinone species. This reduction is ascribed to the effect of the ligand distortion. From the oxygenation studies, it is indicate that Fe(III)-monodentate dianionic catecholate intermediate is the most probable candidate for the direct reactant with O_2. In the CTD model reactions, the ferric ion would serve as a promoter of deprotonation of catecholate monoanion. Further the ferric ion is play an important role in the peroxide complex to give the desired products. These roles of the ferric ion is attributed to its Lewis acidity.

In Chapter V, we discuss the correlation between the EPR parameters and the coordination environments of the non-heme ferric complexes. Unfortunately, we cannot afford the general theoretical correlation between them, but find an empirical rule. The EPR spectra of the non-heme ferric complexes are influenced by the exogenous ligand coordination. The perturbation of one exogenous oxyanion ligand coordination gives the EPR spectrum change from E/D~1/3 to E/D~0.30, of two exogenous oxyanion ligands to E/D~0.20, and of two exogenous oxyanion ligands one of which binds directly to the ferric ion but the other is in the vicinity of the ferric ion to E/D~0.13. The theoretical explanation of this correlation is left as a future subject.

Finally, the author wishes the conclusions and suggestions in this thesis to contribute to develop an important area in the bioinorganic chemistry.

References

1) G. Rotillo Ed., 'Superoxide and Superoxide Dismutase in Chemistry, Biology and Medicine.', Elsevier/North Holland Biochemical Press, Amsterdam (1986)

2) For recent reviews of these enzymes, see
a) M. Nozaki, *Top.Curr.Chem.*, 78, 145 (1979); b) L. Que, Jr., *Adv. Inorg.Biochem.*, 5, 167 (1983); c) L. Que, Jr., *J.Chem.Educ.*, 62, 938 (1985)

3) S. Ahmad, J. D. McCallum, A. K. Shiemke, E. H. Appelman, T. M. Loehr, and J. Sanders-Loehr, *Inorg.Chem.*, **27**, 2230 (1988)

4) L. Que, Jr., R. C. Kolanczyk, and L. S. White, *J.Am.Chem.Soc.*, **109**, 5373 (1987)

5) M. Gerloch and F. E. Mabbs, *J.Chem.Soc.(A)*, 1900 (1967)

6) L. Casella, M. Gullotti, A. Pintar, L. Messori, A. Rockenbauer, and M. Győr, *Inorg.Chem.*, **26**, 1031 (1987)

7) a) J. S. Griffith, 'The Theory of Transition Metal Ions', Cambridge University Press, Cambridge (1961); b) H. Kamimura, S. Sugano, and Y. Tanabe, 'Ligand Field Theory and Its Applications', Syokabo, Tokyo (1969)

8) E. S. Kirkpatrick, K. A. Muller, and R. S. Rubins, *Phys.Rev.*, **135**, A86 (1964)

9) D. J. E. Ingram, 'Spectroscopy at Radio and Microwave Frequencies', Butterworths Scientific Publications Ltd., London (1967)

10) F. J. Yost and I. Fridovich, *J.Biol.Chem.*, **248**, 4905 (1973)

11) a) D. Ringe, G. A. Petsko, F. Yamakura, K. Suzuki, and D. Ohmori, *Proc.Natl.Acad.Sci.USA*, **80**, 3879 (1983); b)W. C. Stallings, T. B. Powers, K. A. Pattridge, J. A. Fee, and M. L. Ludwig, *Proc.Natl.Acad.Sci.USA*, **80**, 3884 (1983)

12) B. L. Stoddard, P. L. Howell, D. Ringe, and G. A. Petsuko, *Biochem.*, **29**, 8885 (1990)

13) a) C. Bull and J. A. Fee, *J.Am.Chem.Soc.*, **107**, 3295 (1985); b) D. M. Dooley, J. L. Karas, T. F. Jones, C. E. Cote, and S. B. Smith, *Inorg.Chem.*, 4761 (1986)

14) C. Bull, G. J. McClune, and J. A. Fee, *J.Am.Chem.Soc.*, **105**, 5290 (1983)

15) a) B. Halliwell, *FEBS Lett.*, **56**, 34 (1975); b) G. J. McClune, J. A. Fee, G. McCluskey, and J. T. Groves, *J.Am.Chem.Soc.*, **99**, 5220 (1977); c) R. F. Pasternack and B. Halliwell, *J.Am.Chem.Soc.*, **101**, 1026 (1979); d) J. Diguiseppi and I. Fridovich, *Arch.Biochem.Biophys.*, **203**, 145 (1980); e) J. Butler and B. Halliwell, *ibid.*, **218**, 174 (1982); f) D. Solomon, P. Peretz, and M. Fraggl, *J.Phys.Chem.*, **86**, 1842 (1986); g) C. Bull, J. A. Fee, P. O'Neill, and E. M. Fielden, *Arch.Biochem. Biophys.*, **215**, 551 (1982); h) G. Minotti and S. D. Aust, *Arch. Biochem.Biophys.*, **253**, 257, (1987); i) T. Nagano, T. Hirano, and M. Hirobe, *J.Biol.Chem.*, **264**, 9243 (1989)

16) K. L. Cheng and P. F. Lott, *Anal.Chem.*, **28**, 462 (1956)

17) A. Ringbom, S. Siitonen, and B. Saxen, *Anal.Chem.*, **16**, 541 (1957)

18) C. Walling, M. Kurz, and H. J. Schugar, *Inorg.Chem.*, **9**, 931 (1970)

19) Y. Ilan and G. Czapski, *Biochim.Biophys.Acta*, **498**, 386 (1977)

20) K. C. Francis, D. Cummins, and J. Oakes, *J.Chem.Soc.Dalton Trans.*, 493 (1985)

21) M. D. Lind and J. L. Hoard, *Inorg.Chem.*, **3**, 34 (1964)

22) G. Schwarzenbach and J. Heller, *Helv.Chim.Acta*, **576**, 576 (1951)

23) P. N. Balasubramanian and T. C. Bruice, *J.Am.Chem.Soc.*, **106**, 5495 (1986)

24) J. C. Evans, *J.Chem.Soc.,Dalton Trans.*, 682 (1969)

25) E. McCandlish, A. R. Mikszotal, M. Nappa, Q. Sprenger, J. S. Valentine, J. D. Strong, and T. G. Spiro, *J.Am.Chem.Soc.*, **102**, 4268 (1980)

26) R. Guillard, J. M. Latour, C. Lecomte, J. C. Marchon, J. Protas, D. Ripoll, I*norg.Chem.*, **17**, 1228 (1978)

27) R. B. VanAtta, C . E. Strouse, L. K. Hanson, and J. S. Valentine, *J.Am.Chem.Soc.*, **109,** 1425 (1987)

28) C. Djordjevic, S. A. Craig, and E. Sinn, *Inorg.Chem.*, **24**, 1281 (1985)

29) B. Charrier, Th. Dibold, and R. Weiss, *Inorg.Chim.Acta*, **19**, 157 (1976)

30) S. Yamada, 'The Structure of Coordination Compounds', Kagakudohjin, Kyoto (1980)

31) P. F. Knowles, J. F. Gibson, F. M. Pick, and R. C. Bray, *Biochem.J.*, **111**, 53 (1969)
32) M. R. Green, H. A. O. Hill, and D. R. Turner. *FEBS Lett.*, **103**, 176 (1979)
33) G. C. Wagner, I. C. Gunslus, M. Y. R. Wang, and B. M. Hoffman, *J.Biol.Chem.*,**256**, 6266 (1981)
34) T. Yonetani, H. Yamamoto, and T. Iizuka, *J.Biol.Chem.*, **249**, 2168 (1974)
35) O. Hayaishi, M. Katagiri, and S. Rothberg, *J.Am.Chem.Soc.*, **77**, 5450 (1955)
36) D. H. Ohlendorf, J. D. Lipscomb, and P. C. Weber, *Nature*, **336**, 403 (1988)
37) C. Bull, D. P. Ballou, and S. Ohtsuka, *J.Biol.Chem.*, **256**, 12681 (1981)
38) L. Que, Jr., J. D. Lipscomb, R. Zimmermann, E. Münck, N. R. Orme-Johnson, and W. H. Orme-Johnson, *Biochim.Biophys.Acta*, **452**, 320 (1976)
39) J. W. Whittaker, J. D. Lipscomb, T. A. Kent, and E. Münck, *J.Biol.Chem.*, **259**, 4466 (1984)
40) T. A. Kent, E. Münck, J. W. Pyrz, J. Widom, and L.Que, Jr.,*Inorg.Chem.*, **26**, 1402 (1987)
41) T. A. Walsh, D. P. Ballou, R. Mayer, and L. Que, Jr., *J.Biol.Chem.*, **258**, 14422 (1983)
42) L. Que, Jr., J. D. Lipscomb, E. Münck, and J. M. Wood, *Biochim.Biophys.Acta*, **485**, 60 (1977)
43) a) M. G. Weller and U. Weser, *J.Am.Chem.Soc.*, **104**, 3752 (1982)
b)M. G. Weller and U. Weser, *Inorg.Chim.Acta*, **107**, 243 (1985)
44) T. Funabiki, A. Mizoguchi, T. Sugimoto, S. Tada, M. Tsuji, H. Sakamoto, and S. Yoshida, *J.Am.Chem.Soc.*, **108**, 2921 (1986)
45) D. D. Cox and L. Que, Jr., *J.Am.Chem.Soc.*, **110**, 8085 (1988)
46) a) T. Funabiki, H. Sakamoto, S. Yoshida, and K. Tarama, *J.Chem.Soc.,Chem.Commun.*, 754 (1979); b) T. Funabiki, S. Tada, T. Yoshioka, M. Takano, and S. Yoshida, *ibid*, 1699 (1986); c) T. Funabiki, T. Konishi, S. Tada, and S. Yoshida, *Chem.Lett.*, 1803 (1987)

47) H. G. Jang, D. D. Cox, and L. Que, Jr., *J.Am.Chem.Soc.*, **113**, 9200 (1991)
48) S. Fujii, H. Ohya-Nishiguchi, and N. Hirota, "Dioxygen Activation and Homogenous Catalytic Oxidation", L. I. Simándi, Ed., Elsevier, Amsterdam, 321 (1991)
49) a) R. B. Lauffer, R. H. Heistand II, and L. Que, Jr., *J.Am.Chem. Soc.*, **1031**, 3947 (1981); b) R. H. Heistand II, R. B. Lauffer, E. Fikrig, and L. Que, Jr., *J.Am.Chem.Soc.*, **104**, 2789 (1982)
50) D. D. Cox, S. J. Benkovic, L. M. Bloom, F. C. Bradley, M. J. Nelson, L. Que, Jr., and D. E. Wallick, *J.Am.Chem.Soc.*, **110**, 2026 (1988)
51) a) V. H. Schulze and W. Flaig, *Ann*, **573**, 231 (1952); b) R. R. Grinstead, Buichem., 3, 1308 (1964); c) F. R. Hewgill and S. L. Lee, J.Chem.Soc.,C, 2080 (1969); d) A. Nishinaga, T. Itahara, and T. Matsuura, *Bull.Chem.Soc.Jpn.*, **47**, 1811 (1974)
52) R. H. Heistand II, A. L. Roe, and L. Que, Jr., *Inorg.Chem.*, **21**, 676 (1982)
53) R. B. Lauffer, R. H. Heistand II, and L. Que, Jr., *Inorg.Chem.*, **22**, 50 (1983)
54) A. M. Orville and J. D. Lipscomb, *J.Biol.Chem.*, **264**, 8791 (1989)
55) a) S Muto and T. C. Bruice, *J.Am.Chem.Soc.*, **102**, 7559 (1980); b) S. Muto and T. C. Bruice, *ibid.*, **104**, 2284 (1982)
56) a) A. Nishinaga, H. Tomita, T. Shimizu, and T. Matsuura, *J.Am. Chem.Soc.*, 100, 1821 (1978); b) A. Nishinaga, H. Tomita, K. Nishizawa, T. Matsuura, S. Ooi, and K. Hirotsu, *J.Chem.Soc.,Dalton Trans.*, 1504 (1981)
57) P. Barbaro, C. Bianchini, C. Mealli, and A. Meli, *J.Am.Chem.Soc.*, **113**, 3181 (1991)
58) a) A. Nishinaga, *Kagaku*, **38**, 740 (1983); b) A. Nishinaga, 'A Book of Abstract. The 1984 International Chemical Congress of Pacfic Basin Societies.',04B04 (1984)
59) T. Funabiki, H. Kojima, M. Kaneko, T. Inoue, T. Yoshioka, T. Tanaka, and S. Yoshida, *Chem.Lett.*, 2143 (1991)
60) A. E. True, A. M. Orville, L. L. Pearce, J. D. Lipscomb, and L. Que, Jr., *Biochem.*, **29**, 10847 (1990)

61) T. Castner, Jr., G. S. Newell, W. C. Holton, and C. P. Slichter, *J.Chem.Phys.*, **32**, 668 (1960)

62) a) J. S. Griffith, *Mol.Phys.*, **8**, 213 (1964); b) J. S. Griffith, *Mol.Phys.*, **8**, 217 (1964)

63) H. H. Wickman, M. P. Klein, and D. A. Shirley, *J.Chem.Phys.*, **42**, 2113 (1965)

64) M. Gerloch, J. Lewis, and R. C. Slade, *J.Chem.Soc..A*, 1422 (1969)

65) R. D. Dowsing and J. F. Gibson, *J.Chem.Phys.*, **50**, 294 (1969)

66) R. Aasa, *J.Chem.Phys.*, **52**, 3919 (1970)

67) G. Lang, R. Aasa, K. Garbett, and R. J. P. Williams, *J.Chem.Phys.*, **55**, 4539 (1971)

68) W. V. Sweeney, D. Coucouvanis, and R. E. Coffman, *J.Chem. Phys.*, **59**, 369 (1973)

69) W. E. Blumberg, "Magnetic Resonance in Biological Systems", A. Ehrenberg, B. G. Malmstrom, and T. Vänngard Eds., Pergamon Press, New York (1967), 119

70) a) H. Yamatera, *Bull.Chem.Soc.Jpn.*, **31**, 95 (1958); b) C. E. Schaffer and C. K. Jorgensen, *Mol.Phys.*, **9**, 401 (1965); c) R. G. Woolley, *Mol.Phys.*, **42**, 703 (1981)

71) K. Fukui, H. Ohya-Nishiguchi, and N. Hirota, *Mol.Phys.*, **71**, 1269 (1990)

72) W. E. Blumberg and W. E. Peisach, *J.Adv.Chem.Ser.*, **100**, 271 (1971)

73) J. Peisach, W. E. Blumberg, and A. D. Alder, *Ann.N.Y.Acad.Sci.*, **206**, 310 (1973)

74) J. S. Griffith, *Proc.R.Soc.London,Ser.A*, **235A**, 23 (1956)

75) J. S. Griffith, *Biopolymers, Symp.*, **1**, 35 (1964)

76) a)M. Kotani, *Suppl.Prog.Theor.Phys.*, **17**, 4 (1961); b) M. Kotani, *Rev.Mod.Phys.*, **35**, 717 (1963); c) M. Kotani, *Biopolymers, Symp.*, **1**, 67 (1964)

77) M. Weissbluth, *Struc.Bonding (Berlin)*, **2**, 1 (1967)

78) C. P. S. Taylor, *Biochim.Biophys.Acta*, **491**, 137 (1977)

79) T. L. Bohan, *J.Mag.Reson.*, **26**, 109 (1977)

80) G. Palmer, 'Iron Porphyrins', A. B. P. Lever and H. B. Gray Eds., Addison-Wesley (1983)